




# SIRT2 negatively regulates the cGAS-STING pathway by deacetylating G3BP1

Yutong Li<sup>1</sup>, Juntao Bie<sup>1</sup>, Chen Song<sup>1</sup>, Yunfei Li<sup>2</sup>, Tianzhuo Zhang<sup>1</sup>, Haishuang Li<sup>3</sup>, Long Zhao<sup>4</sup> , Fuping You<sup>2,\*</sup>  & Jianyuan Luo<sup>1,5,\*\*</sup> 

## Abstract

SIRT2, a cytoplasmic member of the Sirtuin family, has important roles in immunity and inflammation. However, its function in regulating the response to DNA virus infection remains elusive. Here, we find that SIRT2 is a unique regulator among the Sirtuin family that negatively modulates the cGAS-STING-signaling pathway. SIRT2 is down-regulated after Herpes simplex virus-1 (HSV-1) infection, and SIRT2 deficiency markedly elevates the expression levels of type I interferon (IFN). SIRT2 inhibits the DNA binding ability and droplet formation of cGAS by interacting with and deacetylating G3BP1 at K257, K276, and K376, leading to the disassembly of the cGAS-G3BP1 complex, which is critical for cGAS activation. Administration of AGK2, a selective SIRT2 inhibitor, protects mice from HSV-1 infection and increases the expression of IFN and IFN-stimulated genes. Our study shows that SIRT2 negatively regulates cGAS activation through G3BP1 deacetylation, suggesting a potential antiviral strategy by modulating SIRT2 activity.

**Keywords** acetylation; cGAS; G3BP1; innate immunity; SIRT2

**Subject Categories** Microbiology, Virology & Host Pathogen Interaction; Post-translational Modifications & Proteolysis; Signal Transduction

**DOI** 10.15252/embr.202357500 | Received 16 May 2023 | Revised 25 September 2023 | Accepted 4 October 2023 | Published online 23 October 2023

**EMBO Reports (2023) 24: e57500**

## Introduction

Innate immunity is the first line of defense to stand against viral infections via sensing different molecular patterns from viruses by various germline-encoded pattern recognition receptors (PRRs) and subsequently producing pro-inflammatory cytokines (Akira *et al*, 2006). Cyclic GMP-AMP synthase (cGAS) is a crucial cytoplasmic PRR that detects foreign DNA from pathogen infections, such as DNA viruses and retroviruses (Sun *et al*, 2013). Activated cGAS

catalyzes the synthesis of cyclic GMP-AMP (cGAMP) from ATP and GTP, which functions as the second messenger to activate the endoplasmic reticulum adaptor stimulator of interferon genes (STING) (Wu *et al*, 2013). STING then translocates to the Golgi apparatus to activate TANK-binding kinase 1 (TBK1) (Sun *et al*, 2009; Zhang *et al*, 2019), leading to the phosphorylation of the transcription factor interferon regulatory factor 3 (IRF3), and the production of type I IFNs (Fitzgerald *et al*, 2003). Alternatively, STING can also activate NF- $\kappa$ B to drive the transcription of pro-inflammatory cytokines such as TNF and IL-1 (Yum *et al*, 2021).

The innate immune responses are well-organized and tightly regulated at different levels to efficiently defend against pathogens while avoiding excessive tissue damage. Ras GTPase-activating protein-binding protein 1 (G3BP1), a central component of stress granules (SGs), required for SG assembly and dynamics (Yang *et al*, 2020a), has been demonstrated to play a crucial role in regulating innate immune signaling, including the cGAS-STING pathway (Liu *et al*, 2019) and the RIG-I-MAVS pathway (Kim *et al*, 2019; Yang *et al*, 2019). G3BP1 promotes cGAS-mediated IFN production by physically interacting with cGAS, and forming a giant complex that facilitates DNA sensing and oligomerization of cGAS (Liu *et al*, 2019; Zhao *et al*, 2022).

SIRT2, a cytoplasm-located NAD<sup>+</sup>-dependent lysine deacetylase, regulates multiple cellular processes, including cell cycle progression (Dryden *et al*, 2003; Kim *et al*, 2011), energy metabolism (Jing *et al*, 2007; Hamaidi *et al*, 2020), oxidative stress response (Wang *et al*, 2007; Xu *et al*, 2014), and programmed cell death (Peck *et al*, 2010). Recent studies have discovered that SIRT2 might be an essential mediator of the host immune response to infections and the onset of inflammation (Cheng *et al*, 2018; Gogoi *et al*, 2018; Piracha *et al*, 2018; Bhaskar *et al*, 2020; Wan *et al*, 2021). SIRT2 translocates to the chromatin and deacetylates histone H3 at lysine 18 after *Listeria* infection, modulating the expression of a set of genes necessary for bacterial replication (Eskandarian *et al*, 2013; Pereira *et al*, 2018). SIRT2 directly binds to and deacetylates p65, the subunit of NF- $\kappa$ B, inhibiting the activation of NF- $\kappa$ B as well as

1 Department of Medical Genetics, Center for Medical Genetics, School of Basic Medical Sciences, Peking University Health Science Center, Beijing, China

2 Department of Immunology, School of Basic Medical Sciences, Beijing Key Laboratory of Tumor Systems Biology, Institute of Systems Biomedicine, Peking University Health Science Center, Beijing, China

3 Department of Pathology, School of Basic Medical Sciences, Peking University Third Hospital, Peking University Health Science Center, Beijing, China

4 Department of Gastroenterological Surgery, Peking University People's Hospital, Beijing, China

5 Beijing Key Laboratory of Protein Posttranslational Modifications and Cell Function, Department of Biochemistry and Biophysics, School of Basic Medical Sciences, Peking University Health Science Center, Beijing, China

\*Corresponding author. Tel: +86 18518590080; E-mail: fupingyou@bjmu.edu.cn

\*\*Corresponding author. Tel: +86 10 82805861; E-mail: luojianyuan@bjmu.edu.cn

the transcription of numerous pro-inflammatory cytokines (Zhang & Chi, 2018; Rothgiesser *et al*, 2019). SIRT2 also negatively regulates the NLRP3 inflammasome assemble by deacetylating NLRP3, leading to the reduced production of IL-1 $\beta$  and cleaved caspase 1 (He *et al*, 2020). However, whether SIRT2 participates in regulating the immune response against DNA viruses remains unclear.

In this study, we show that SIRT2 inhibits cGAS activation through the direct interaction with and deacetylation of G3BP1. Treating mice with the selective SIRT2 inhibitor AGK2 protects them from HSV-1 infection by increasing IFN levels and the expression of IFN-stimulated genes. Our study reveals a novel role of SIRT2 in negatively regulating cGAS activation via G3BP1 deacetylation, suggesting a potential antiviral strategy by modulating SIRT2 activity.

## Results

### SIRT2 negatively regulates IFN- $\beta$ production upon HSV-1 infection

To explore the potential role of Sirtuins in response to HSV-1 infection, we knocked down all Sirtuin members in HeLa cells followed by HSV-1 infection and found that only SIRT2 knockdown significantly increased IFN- $\beta$  expression (Fig 1A), which was further confirmed in THP-1 cells (Fig EV1A–C). We next generated SIRT2 stably knockdown HeLa and THP-1 cell lines (Fig EV1D), and found that deficiency of SIRT2 significantly enhanced IFN- $\beta$  and ISGs expression induced by HSV-1 infection (Figs 1B and EV1E). A similar result was obtained in 4T1 cells, a murine cell line, indicating that the function of SIRT2 in antiviral response was conserved between humans and mice (Fig EV1F). On the contrary, overexpression of SIRT2 severely inhibited the induction of IFN- $\beta$  (Fig 1C) and IFN-stimulated genes (ISGs) (Fig EV1G) by HSV-1 infection. Consistently, the luciferase assay revealed that SIRT2 repressed the activation of IFN- $\beta$  promoter which was cloned into the luciferase-expressing plasmid via analysis of the luciferase activity, while the enzymatic inactivated mutant of SIRT2 (Eskandarian *et al*, 2013) failed to exhibit this effect (Fig 1D and E). In addition, the luciferase assay also showed that lack of SIRT2 increased the IFN- $\beta$  secretion of THP-1 cells after HSV-1 infection (Fig EV1H). AGK2 is a selected SIRT2 inhibitor, which has shown a potent effect against pathogens such as hepatitis B virus (Bhaskar *et al*, 2020) and *M. tuberculosis* (Yu *et al*, 2018). We pretreated HeLa or THP-1 cells with AGK2, and found that inhibition of SIRT2 strongly elevated IFN- $\beta$  production (Fig 1F). However, such effect was restrained in SIRT2 knockdown THP-1 cells (Fig EV1I), indicating that AGK2 indeed functioned through SIRT2 for its antiviral effect. However, neither SIRT2 knockdown nor AGK2 treatment promoted IFN- $\beta$  production after vesicular stomatitis virus (VSV), an RNA virus that can strongly stimulate RNA-sensing pathway activation, infected in THP-1 cells (Fig EV1J and K). Taken together, these results demonstrated that SIRT2 was a novel suppressor for HSV-1 infection-induced IFN- $\beta$  production.

Interestingly, SIRT2 was the only Sirtuin member that progressively decreased upon HSV-1 infection at both protein and mRNA levels (Figs 1G and EV1L). In addition, the expression level of SIRT2 was reduced in an HSV-1 dose-dependent manner (Fig EV1M). We further confirmed this result *in vivo* by infecting C57BL/6 mice with

HSV-1 ( $5 \times 10^6$  PFU) and collected the blood, liver, and brain tissues, finding that both mRNA and protein levels of SIRT2 decreased upon HSV-1 infection (Figs 1H and I, and EV1N and O). The analysis of the GEO database also showed that the SIRT2 mRNA level was reduced in the liver and brain tissues of HSV-1-infected mice (Fig EV1P). Additionally, we found that herring testis DNA (HT-DNA) transfection could also induce SIRT2 decrease in both mRNA and protein levels (Fig EV1Q). Considering that both HSV-1 and HT-DNA can induce IFN- $\beta$  secretion, the data from GEO database showed that SIRT2 expression level reduced in IFN-treated cells, indicating that SIRT2 can be down-regulated by IFN- $\beta$  (Fig EV1R). We then confirmed that both protein and mRNA levels of SIRT2 were reduced in an IFN- $\beta$  dose-dependent manner (Fig 1J and K). Furthermore, the inhibitor of JAK–STAT pathway, Ruxolitinib, was able to partially block the down-regulation of SIRT2 after HSV-1 infection (Fig EV1S and T). Since HSV-1 infection could induce elevated HIF-1 $\alpha$  expression due to hypoxia and type I IFN (Yeh *et al*, 2018; Rao & Suvas, 2019), and SIRT2 could be transcriptionally repressed by HIF-1 $\alpha$  (Krishnan *et al*, 2012). We validated that HSV-1 infection could promote HIF-1 $\alpha$  protein levels while down-regulating SIRT2 expression (Fig EV1U). Besides, we treated cells with CoCl<sub>2</sub> that was able to strongly inhibit the activity of the prolyl hydroxylases (PHDs) and stabilized HIF-1 $\alpha$  (Muñoz-Sánchez & Cháñez-Cárdenas, 2019). The results showed that both protein and mRNA levels of SIRT2 decreased after CoCl<sub>2</sub> treatment (Fig EV1V and W). Notably, knockdown of HIF-1 $\alpha$  was partially able to prevent SIRT2 reduction (Figs 1L and EV1X). In total, these data indicated that SIRT2 is down-regulated upon HSV-1 infection, which is partially related to HIF-1 $\alpha$ .

### SIRT2 inhibits the cGAS-STING pathway

Since the cGAS-STING pathway is primarily activated by DNA virus infection, it is reasonable to speculate that SIRT2 suppresses HSV-1-induced IFN- $\beta$  production by regulating the cGAS-STING pathway. As cGAS and STING are typically transcriptionally silenced in cancer cell lines (Qiao *et al*, 2020), we first confirmed the expression patterns of cGAS and STING in HeLa and THP-1 cells, which were the main cell lines used in this study (Fig EV2A). Additionally, we validated that loss of cGAS prevented IFN- $\beta$  production induced by HSV-1 infection (Fig EV2B). Furthermore, we transfected HT-DNA or interferon stimulatory DNA (ISD), both of which are substrates of cGAS, into SIRT2-deficient cells. The results revealed that loss of SIRT2 significantly augmented DNA-induced IFN- $\beta$  and ISGs production (Figs 2A and EV2C and D). In contrast, SIRT2 overexpression suppressed DNA-stimulated IFN- $\beta$  expression (Fig 2B). However, SIRT2 knockdown had little influence on the production of IFN- $\beta$  induced by poly(I:C), a mimic for RNA virus infection (Kato *et al*, 2006) (Fig EV2E). We next examined the phosphorylation levels of TBK1 and IRF3, which serve as the downstream effectors of activated cGAS. We confirmed that HSV-1-induced activation of TBK1 and IRF3 was cGAS dependent (Fig EV2F). By knocking down all Sirtuin members using siRNAs, we found that only SIRT2 deficiency strongly promoted the phosphorylation levels of TBK1 and IRF3 induced by HSV-1 (Fig 2C). The result was further confirmed in SIRT2 stably knocked-down THP-1 cells (Figs 2D and E, and EV2G). In contrast, overexpression of SIRT2 reduced the phosphorylation levels of TBK1 and IRF3 in response to HSV-1 infection

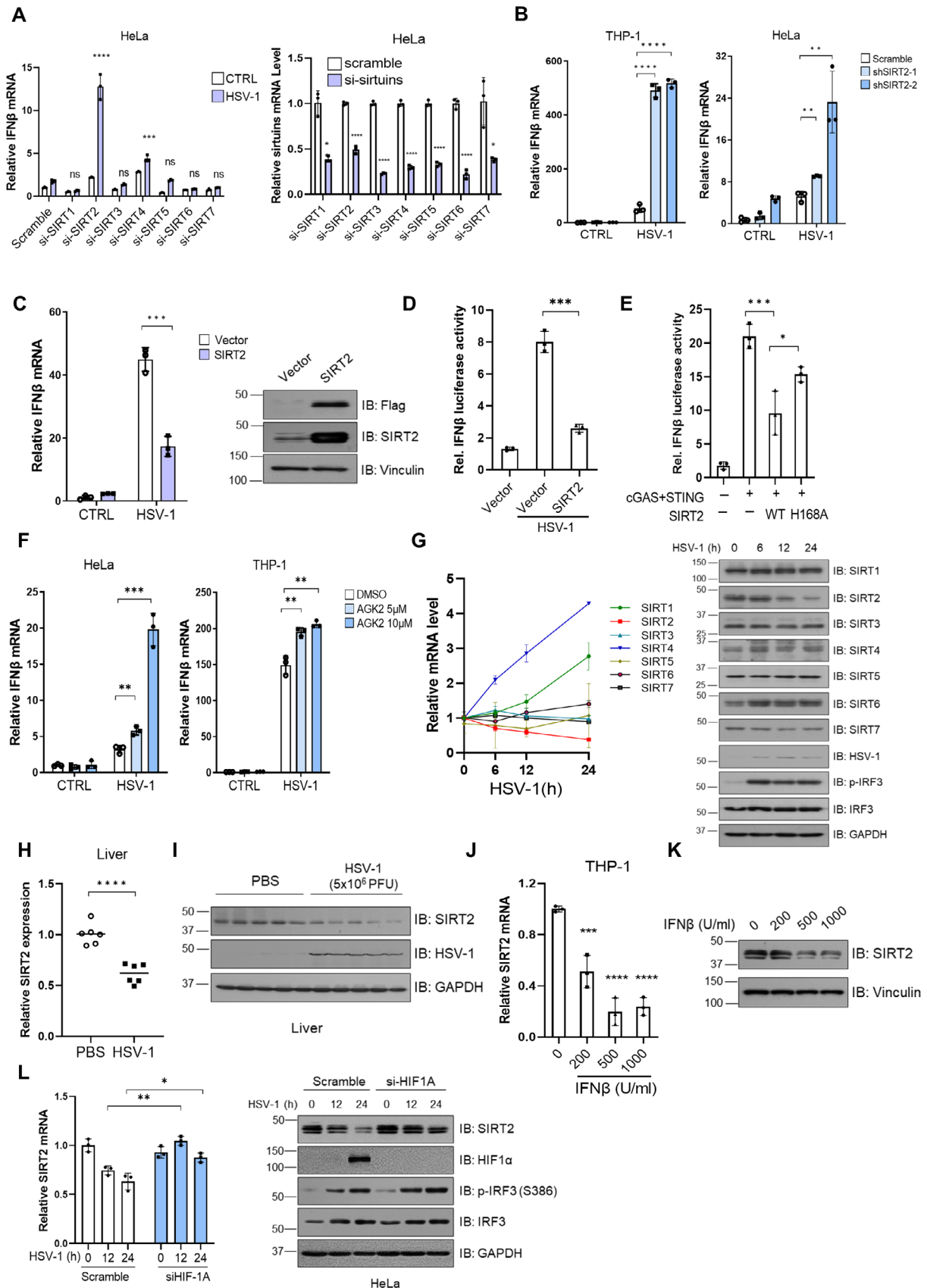


Figure 1.

**Figure 1. SIRT2 is down-regulated after HSV-1 infection to promote type I IFN production.**

- A qPCR analysis of *Ifnb1* mRNA (left) or *sirt1-sirt7* mRNA (right) in HeLa cells transfected with siRNA against SIRT1 to SIRT7 for 48 h followed by HSV-1 infection (MOI = 1) for another 12 h ( $n = 3$ , biological replicates).
- B qPCR analysis of *Ifnb1* mRNA in SIRT2-deficient THP-1 (left) or HeLa cells (right) infected with HSV-1 (MOI = 1) for 6 h ( $n = 3$ , biological replicates).
- C qPCR analysis of *Ifnb1* mRNA in SIRT2 stably overexpressed HeLa cells infected with HSV-1 (MOI = 1) for 12 h (left;  $n = 3$ , biological replicates). Immunoblot analysis of SIRT2 overexpressed HeLa cells (right).
- D Luciferase assay analysis of IFN- $\beta$  promoter activity in SIRT2 stably overexpressed HeLa cells infected with HSV-1 (MOI = 1) for 4 h ( $n = 3$ , biological replicates).
- E The luciferase assay analysis of IFN- $\beta$  promoter activity in SIRT2 (wild-type) or SIRT2 (H168A mutant)-transfected HEK293T cells that exogenously expressed cGAS and STING ( $n = 3$ , biological replicates).
- F qPCR analysis of *Ifnb1* mRNA in AGK2 pretreated HeLa (left) or THP-1 cells (right) infected with HSV-1 (MOI = 1) for 6 h ( $n = 3$ , biological replicates).
- G qPCR analysis of *sirt1-sirt7* mRNA expression (left) or immunoblot of SIRT1-SIRT7 protein levels (right) in HeLa cells infected with HSV-1 (MOI = 1) for indicated time ( $n = 3$ , biological replicates).
- H qPCR analysis SIRT2 mRNA level in the liver tissues of HSV-1 ( $5 \times 10^6$  PFU)-infected C57BL/6 mice after 3 days ( $n = 6$ , biological replicates).
- I Immunoblot of SIRT2 protein level in the liver tissues of HSV-1-infected mice.
- J qPCR analysis of *sirt2* mRNA level in IFN- $\beta$ -treated THP-1 cells at indicated concentrations for 12 h ( $n = 3$ , biological replicates).
- K Immunoblot analysis of SIRT2 protein level in THP-1 cells treated with different amounts of IFN- $\beta$  as indicated for 12 h.
- L qPCR analysis of *sirt2* mRNA level (left) or Immunoblot analysis of SIRT2 protein level (right) in HIF-1 $\alpha$  knockdown HeLa cells infected with HSV-1 (MOI = 1) for indicated time ( $n = 3$ , biological replicates).

Data information: \* $P < 0.05$ , \*\* $P < 0.01$ , \*\*\* $P < 0.001$ , \*\*\*\* $P < 0.0001$ . For (A, C, D, H, and L), the two-tailed unpaired Student's *t*-test was used. For (B, E, F, and J), the one-way ANOVA was used. Bars, mean  $\pm$  SD.

Source data are available online for this figure.

(Fig 2F). However, knockdown of SIRT2 failed to promote the activation levels of TBK1 and IRF3 in VSV-infected THP-1 cells (Fig EV2H). Similar to HSV-1 infection, knockdown of SIRT2 via siRNAs notably increased the phosphorylation levels of TBK1 and IRF3 upon HT-DNA transfection among the Sirtuin family (Fig EV2I). Consistently, the activation levels of TBK1 and IRF3 were elevated in SIRT2 stably knocked-down THP-1 cells, induced by HT-DNA but not poly(I:C) transduction (Figs 2G and EV2J and K). In contrast, SIRT2 overexpression showed inhibitory effects on HT-DNA-induced TBK1 and IRF3 phosphorylation (Fig EV2L). Additionally, inhibition of SIRT2 by AGK2 increased the DNA-stimulated IFN- $\beta$  production (Fig 2H). AGK2 treatment also promoted the phosphorylation levels of TBK1 and IRF3 after HSV-1 or HT-DNA stimulation, but not VSV infection (Figs 2I and EV2M and N).

### SIRT2 suppresses cGAS activity

We further investigated the specific target of SIRT2 in regulating the cGAS-STING pathway. We first treated HeLa cells with cGAMP, the activator of STING. The data revealed that cGAMP induced similar levels of IFN- $\beta$  and the phosphorylation levels of TBK1 and IRF3 in both wild-type and SIRT2-deficient cells (Fig 2J and K), suggesting that SIRT2 regulates the cGAS-STING pathway upstream of STING activation. To confirm this result, we knocked out cGAS in SIRT2 knockdown cells using CRISPR/Cas9 for the experiments. The results showed that loss of cGAS was capable of eliminating the facilitation effect on IFN- $\beta$  production in SIRT2 knockdown cells induced by both HSV-1 and HT-DNA (Figs 3A and EV2O). A similar result was also obtained in AGK2-pretreated cells (Fig EV2P). Furthermore, loss of cGAS also eliminated the elevated phosphorylation levels of TBK1 and IRF3 induced by SIRT2 knockdown (Figs 3B and EV2Q). To further investigate the activity of cGAS in the absence of SIRT2, we detected the production of cGAMP upon DNA stimulation, revealing that loss of SIRT2 notably increased cellular cGAMP concentration in both THP-1 and HeLa cells (Fig 3C). We then transfected biotin-linked ISD into SIRT2 knockdown cells and found that SIRT2 knockdown promoted the interaction between ISD and cGAS (Fig 3D). As cGAS can form liquid-like droplets via phase separation

after binding to DNA, which robustly enhances the production of cGAMP (Du & Chen, 2018), we investigated whether SIRT2 could influence the formation of cGAS foci. The result showed that the lack of SIRT2 or AGK2 pretreatment was able to increase the number of cGAS-foci-positive cells induced by both HSV-1 and ISD (Figs 3E and F, and EV2R–U). Taken together, these results demonstrated that SIRT2 can suppress the activity of cGAS.

### SIRT2 interacts with G3BP1

Next, we investigated whether SIRT2 could directly regulate the acetylation level of cGAS. The result revealed that SIRT2 had negligible influence on the acetylation status of cGAS (Fig 3G), indicating that SIRT2 regulated cGAS in an indirect manner. To study the potential mechanism, we purified SIRT2-interacting proteins from SIRT2-Flag stably expressed HeLa cells. The purified proteins were visualized by silver staining (Fig 4A) and identified by mass spectrometry. SIRT2 interacts with multiple proteins that function in nucleic acid binding and protein complex binding, and many of these interacting proteins are involved in the process of virus infection and participate in the response to virus (Figs 4B and EV3A and B). Among them, G3BP1, which is critical for cGAS activation, was identified in the experiment (Fig EV3C). To confirm the interaction between SIRT2 and G3BP1, we transiently transfected SIRT2 and G3BP1 constructs into HEK293T cells and found that SIRT2 and G3BP1 could be clearly co-immunoprecipitated by each other (Fig EV3D). Furthermore, the endogenous co-immunoprecipitation assay further confirmed their interaction in cells, with KRAS and SQSTM1 being positive interactors for SIRT2 (Jing *et al*, 2017) and G3BP1 (Anisimov *et al*, 2019), respectively (Fig 4C). Meanwhile, the GST-pulldown assay showed that SIRT2 could interact with G3BP1 *in vitro* (Fig EV3E). The direct interaction between SIRT2 and G3BP1 was confirmed by the MicroScale Thermophoresis (MST) assay, and the dissociation constant (Kd) was around 80 nM (Fig 4D). Notably, the association of G3BP1 and SIRT2 strikingly decreased under HSV-1 infection (Fig 4E), indicating that the antiviral functions of G3BP1 might require dissociation with SIRT2. In addition, the immunofluorescent staining assay demonstrated that

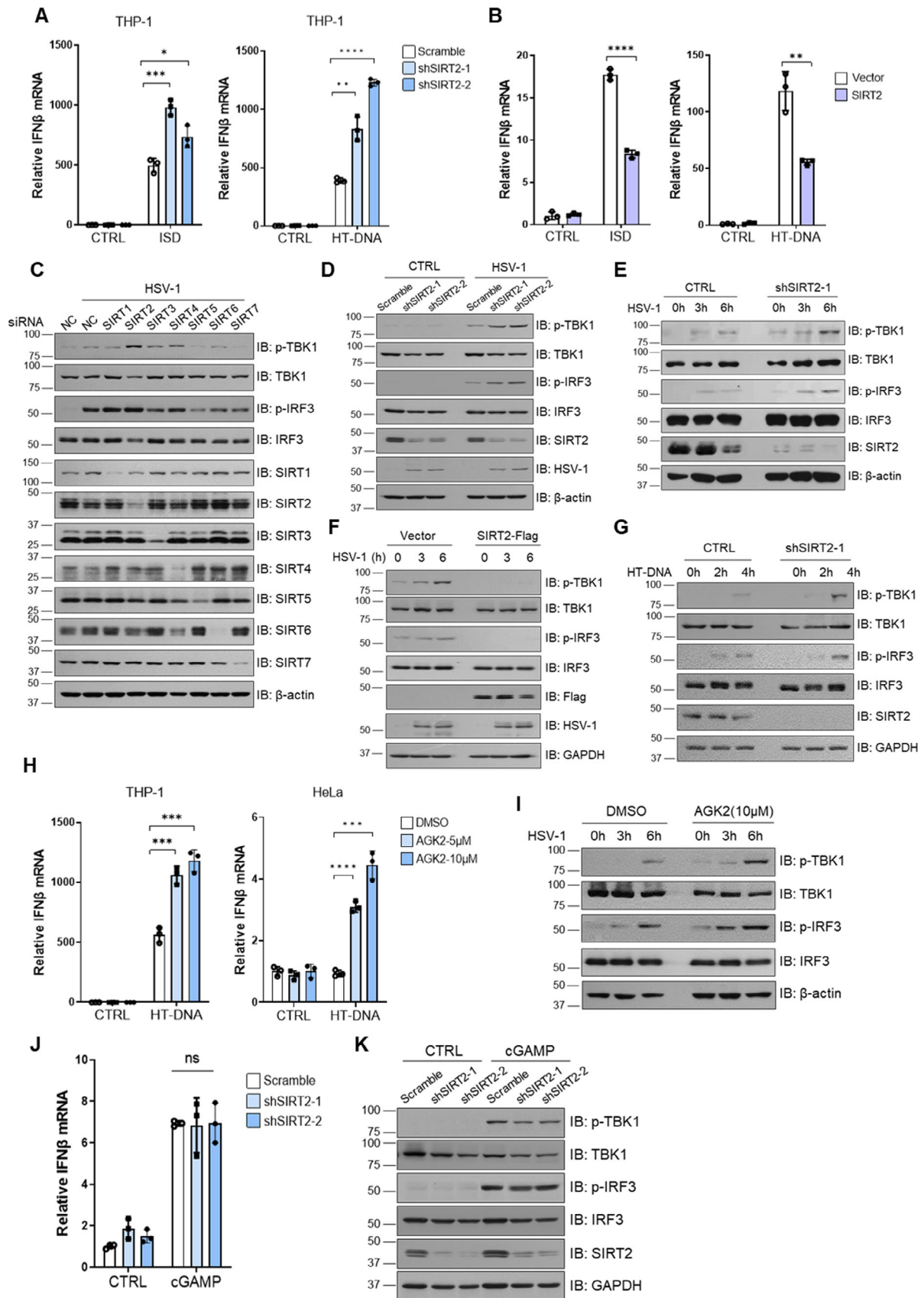


Figure 2.

**Figure 2. SIRT2 negatively regulates the cGAS-STING pathway.**

- A qPCR analysis of *Irfnb1* mRNA in SIRT2 knockdown THP-1 cells transfected with ISD (2 µg/ml, left) or HT-DNA (2 µg/ml, right) for 4 h ( $n = 3$ , biological replicates).
- B qPCR analysis of *Irfnb1* mRNA in SIRT2 stably overexpressed HeLa cells transfected with ISD (2 µg/ml, left) or HT-DNA (2 µg/ml, right) for 6 h ( $n = 3$ , biological replicates).
- C Immunoblot analysis of cGAS signaling in HeLa cells transfected with siRNA against SIRT1 to SIRT7 for 48 h and followed by HSV-1 (MOI = 1) infected for another 6 h.
- D Immunoblot analysis of cGAS signaling in SIRT2 knockdown THP-1 cells infected with HSV-1 (MOI = 1) for 6 h.
- E Immunoblot analysis of cGAS signaling in SIRT2 knockdown THP-1 cells infected with HSV-1 (MOI = 1) for indicated times.
- F Immunoblot analysis of cGAS signaling in SIRT2-overexpressed HeLa cells infected with HSV-1 (MOI = 1) for indicated time.
- G Immunoblot analysis of cGAS signaling in SIRT2 knockdown THP-1 cells transfected with HT-DNA (2 µg/ml) for indicated times.
- H qPCR analysis of *Irfnb1* mRNA in AGK2 pretreated THP-1 (left) or HeLa cells (right) followed by HT-DNA stimulation for 4 h ( $n = 3$ , biological replicates).
- I Immunoblot analysis of cGAS signaling in AGK2 pretreated (10 µM) HeLa cells infected with HSV-1 (MOI = 1) for indicated times.
- J qPCR analysis of *Irfnb1* mRNA in SIRT2 knockdown THP-1 cells treated with cGAMP (1 µg/ml) for 4 h ( $n = 3$ , biological replicates).
- K Immunoblot analysis of cGAS signaling in SIRT2 knockdown THP-1 cells treated with cGAMP (1 µg/ml) for 4 h.

Data information: NS, not significant, \* $P < 0.05$ , \*\* $P < 0.01$ , \*\*\* $P < 0.001$ , \*\*\*\* $P < 0.0001$ . For panel (B), the two-tailed unpaired Student's *t*-test was used. For (A, H, and J), the one-way ANOVA was used. Bars, mean  $\pm$  SD.

Source data are available online for this figure.

SIRT2 scarcely co-localized with G3BP1 in the antiviral droplets (Fig 4F), and was also not present in the cGAS foci after HSV-1 infection (Fig EV3F). In conclusion, the above data demonstrated that SIRT2 directly interacts with G3BP1.

**SIRT2 deacetylates G3BP1**

To investigate whether SIRT2 can deacetylate G3BP1, we first transfected HEK293T cells with increasing amounts of SIRT2 plasmids, finding that G3BP1 acetylation levels progressively decreased (Fig 4G). However, the catalytically inactivated mutant SIRT2-N168A failed to deacetylate G3BP1 in cells (Fig 4H). Besides, the *in vitro* deacetylation assay showed that SIRT2 was able to deacetylate G3BP1 *in vitro*, only when the NAD<sup>+</sup> was presented (Fig 4I). Consistently, the acetylation levels of endogenous G3BP1 were increased in SIRT2-deficient cells (Fig 4J). Also, AGK2 was able to elevate G3BP1 acetylation levels (Fig 4K). Notably, loss of G3BP1 significantly restricted the promotion effects of SIRT2 knockdown on IFN- $\beta$  production as well as TBK1 and IRF3 activation (Fig EV3G and H). All of these results demonstrated that G3BP1 is a novel substrate of SIRT2 for DNA virus infection response.

**G3BP1 is acetylated by CBP**

To investigate the dynamic regulation of G3BP1 acetylation, we first examined the acetylation levels of G3BP1 upon virus infection. The acetylation levels of G3BP1 gradually increased after HSV-1 infection (Fig 5A). We next identified the acetyltransferase of G3BP1 by examining several common histone acetyltransferases (HATs). The result showed that only CREB-binding protein (CBP) significantly increased the acetylation levels of G3BP1 (Fig 5B). In agreement with this, the deficiency of CBP lowered the G3BP1 acetylation levels (Fig 5C). Furthermore, we found that CBP was also recruited to the cytosolic droplets along with cGAS in response to HSV-1 infection or ISD stimulation (Figs 5D and EV3I), indicating a potential role of CBP in regulating cGAS activity that was opposite to SIRT2. Thus, we knocked down CBP by siRNAs, which showed that CBP deficiency inhibited both IFN- $\beta$  transcription and the phosphorylation levels of TBK1 and IRF3 stimulated by HSV-1 (Fig EV3J and K).

We next purified the hyperacetylated G3BP1 from cells overexpressed CBP to identify the acetylation sites through mass

spectrometry. Two lysine residues (K257 and K376) were identified (Fig 5E, Dataset EV1). We mutated the two sites, along with the other two adjacent lysine residues in the same peptides, in order to avoid masked signals, to arginine (R), which mimicked the hypoacetylation modification. The data demonstrated that each individual mutation of K257, K276, and K376 could reduce G3BP1 acetylation levels (Fig 5F and G). Consistently, the 3KR mutation altogether led to the lowest acetylation levels (Fig 5G and H). Homology analysis indicated that all these three sites were highly conserved residues from *Xenopus tropicalis* to *Homo sapiens* (Fig EV3L). Notably, overexpression of G3BP1 3KQ (lysine- to glutamine-mimicking hyperacetylation) could counteract the inhibition of SIRT2 on cGAS pathway activation (Fig 5I). Altogether, we found that G3BP1 acetylation levels increased after HSV-1 infection, and CBP acetylated G3BP1 at K257, K276, and K376 residues.

**Hyperacetylated G3BP1 facilitates cGAS activation**

To further explore the effect of G3BP1 acetylation on the cGAS-STING-signaling pathway, we generated G3BP1 WT, 3KR, and 3KQ mutants stably expressing HeLa cells. It was reported that G3BP1 and cGAS form a macromolecular complex, and the lack of any domain of G3BP1 would impair their interaction (Liu *et al*, 2019). Therefore, we performed an immunoprecipitation assay to examine the interaction between G3BP1 mutants and cGAS. The results showed that G3BP1 3KQ interacted more strongly with cGAS, while 3KR mutant markedly reduced their interaction (Fig 6A). In addition, overexpression of CBP increased the amounts of endogenous cGAS co-immunoprecipitated by G3BP1 (Fig 6B). A similar result was also obtained in AGK2-treated HeLa cells (Fig 6C).

Since the interaction with G3BP1 was crucial for cGAS activation, we first investigated the effect of G3BP1 acetylation on IFN- $\beta$  production. We deleted endogenous G3BP1 via CRISPR/Cas9 and re-expressed G3BP1 WT, 3KR, and 3KQ mutants in HeLa cells (Fig EV4A). We found that G3BP1 3KQ-rescued cells exhibited a strongly elevated IFN- $\beta$  production level; in contrast, G3BP1 3KR impaired IFN- $\beta$  production in response to HSV-1 or HT-DNA (Fig 6D). However, such effects were unobvious in VSV-infected HeLa cells (Fig EV4B). Consistently, G3BP1 3KQ increased the phosphorylation levels of TBK1 and IRF3, while G3BP1 3KR inhibited their activation after HT-DNA or HSV-1 stimulation but not VSV

infection (Figs 6E and EV4C). Besides, the exogenous overexpression of G3BP1 3KR mutant also significantly diminished IFN- $\beta$  mRNA levels after HSV-1 or HT-DNA stimulations, while G3BP1 3KQ-expressed cells produced more or comparable IFN- $\beta$  with WT

(Fig EV4D). Additionally, G3BP1 3KQ also facilitated the DNA-binding activity of cGAS (Figs 6F and EV4E). Furthermore, we found that knockdown of SIRT2 promoted G3BP1-cGAS foci formation (Fig 6G and H), while CBP deficiency prevented the formation of

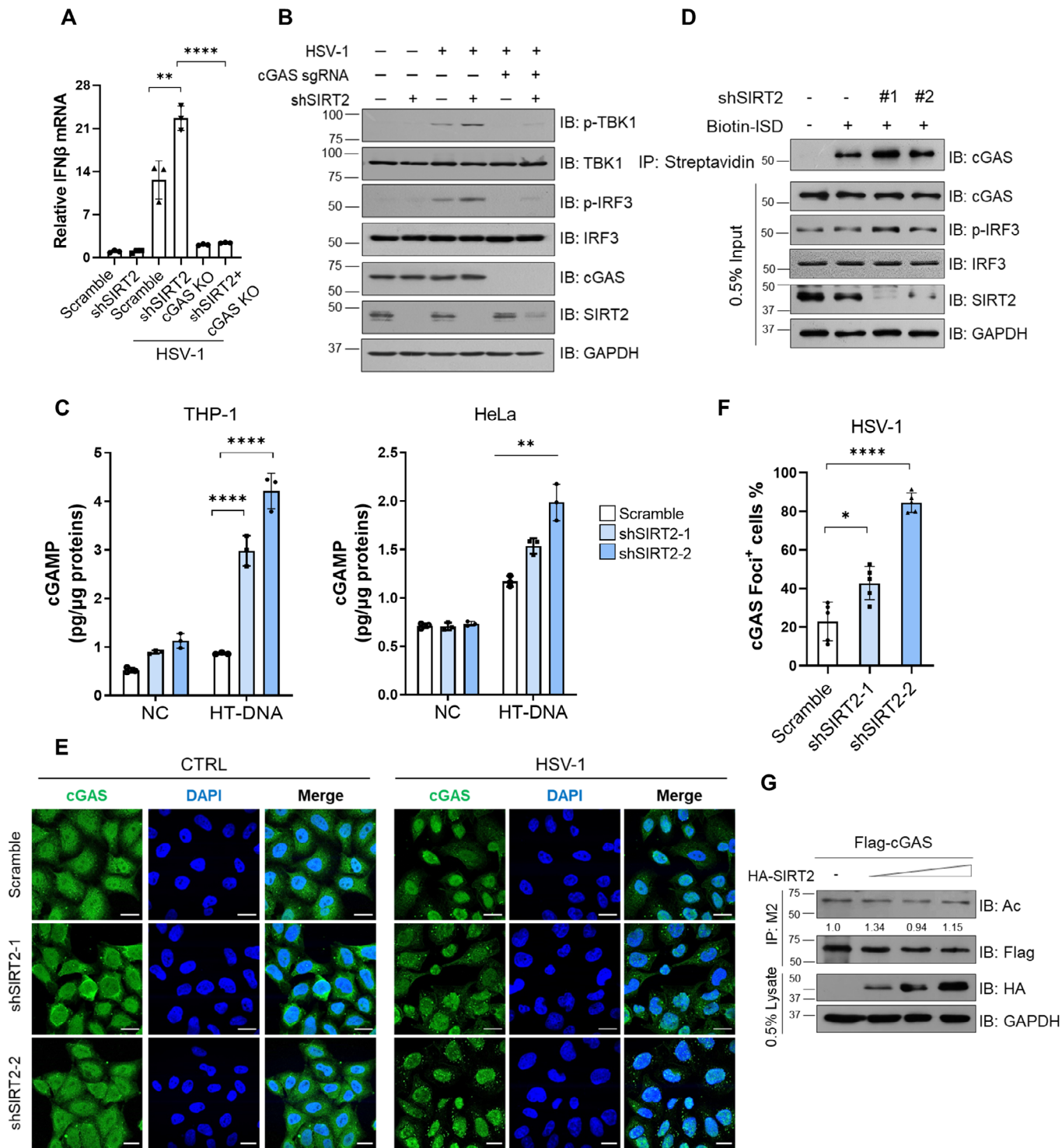


Figure 3.

**Figure 3. SIRT2 inhibits cGAS activation.**

- A qPCR analysis of *Ifnb1* mRNA in cGAS knockout and SIRT2-deficient HeLa cells infected with HSV-1 (MOI = 1) for 12 h ( $n = 3$ , biological replicates).
- B Immunoblot analysis of cGAS signaling in cGAS knockout and SIRT2 knockdown HeLa cells infected with HSV-1 (MOI = 1) for 6 h.
- C Measurement of cGAMP in SIRT2 knockdown THP-1 (left) or HeLa cells (right) transfected with HT-DNA for 3 h. The whole protein concentration was used for normalization ( $n = 3$ , biological replicates).
- D ISD-bound cGAS was enriched by streptavidin magnetic beads in HeLa cells and analyzed by immunoblotting.
- E Representative immunofluorescent staining of cGAS (green) in SIRT2 knocked-down HeLa cells infected with HSV-1 (MOI = 1) for 6 h. Scale bars (bottom right), 20  $\mu\text{m}$ .
- F The percentage of cells stained with cGAS foci was quantified ( $n = 5$ , biological replicates).
- G HEK293T cells were transfected with cGAS and SIRT2 constructs as indicated, and the acetylation level of cGAS was analyzed by immunoblotting assay.
- Data information: \* $P < 0.05$ , \*\* $P < 0.01$ , \*\*\* $P < 0.001$ , \*\*\*\* $P < 0.0001$ . For (A, C, and F), the one-way ANOVA was used. Bars, mean  $\pm$  SD. Source data are available online for this figure.

puncta induced by HSV-1 infection (Fig EV4F and G). Consistently, G3BP1 3KQ promoted cGAS phase separation induced by both HSV-1 and ISD, while G3BP1 3KR had a converse effect (Figs 6I and J, and EV4H and I). In accordance, the *in vitro* phase separation assay showed a similar result (Fig EV4J and K). Taken together, these results demonstrated that hyperacetylated G3BP1 interacted strongly with cGAS and facilitated cGAS activation.

**SIRT2 inhibition alleviates the susceptibility to HSV-1 infection**

Our results on SIRT2 repressing the cGAS-STING pathway led us to hypothesize that inhibition of SIRT2 would have protective antiviral effect *in vitro* and *in vivo*. To test this, we first infected SIRT2 knockdown HeLa cells with GFP-expressing HSV-1 and found that deficiency in SIRT2 inhibited virus replication (Fig 7A). In line with this, the plaque assay demonstrated that SIRT2 deficiency lowered the HSV-1 titers but not the VSV titers in THP-1 cells (Figs 7B and EV5A). The result was further confirmed by the quantification of HSV-1 RNA abundance (Fig 7C). Next, we pretreated cells with AGK2 12 h before HSV-1 infection, finding that AGK2-pretreated cells acquired resistance to HSV-1 but not VSV infection (Figs 7D–F and EV5B). Since SIRT2 was reported to regulate autophagy (Zhao *et al*, 2010), and AGK2 was also reported to induce autophagy or apoptosis, which might be involved in virus clearance (Zhao *et al*, 2010; Li *et al*, 2013), we then validated that the administration

of AGK2 or SIRT2 knockdown in our study had a negligible effect on autophagy (Fig EV5C–F). Besides, neither SIRT2 knockdown nor AGK2 caused obvious damage to the viability of the HSV-1-infected cells (Fig EV5G and H). To explore if the virus clearance effects were related to cGAS pathway, we repeated the experiments in cGAS-deficient cells, finding that loss of cGAS significantly counteracted the effects of SIRT2 knockdown and AGK2 treatment (Fig EV5I and J). Also, we tested HSV-1 multiplication in G3BP1-rescued cells and found that G3BP1 3KQ cells demonstrated a lower virus load while G3BP1 3KR facilitated HSV-1 replication (Fig EV5K and L).

We further administrated mice with AGK2 or DMSO ahead of HSV-1 infection and then quantified HSV-1 RNA abundance in serum and tissues. We found that the HSV-1 mRNA levels reduced in the blood, brain, and liver tissues from AGK2 pretreated mice (Fig 7G), while the co-treatment of RU.521, the specific inhibitor of cGAS (Vincent *et al*, 2017), could counteract the effects of AGK2 (Fig 7H), indicating that AGK2-inhibiting HSV-1 replication *in vivo* requires cGAS. To further confirm the effects of AGK2 were associated with IFN- $\beta$  production, we examined the serum IFN- $\beta$  level via ELISA analysis, and the result showed that AGK2 was able to elevate IFN- $\beta$  production (Fig 7I). Since AGK2 was reported to lower TNF $\alpha$  levels, which might be related to virus clearance (Kim *et al*, 2020), we then tested the TNF $\alpha$  secretion in AGK2-treated mice. The data demonstrated that AGK2 was able to slightly

**Figure 4. SIRT2 interacts with and deacetylates G3BP1.**

- A Mass spectrometry analysis of SIRT2-interacted proteins. Stably expressing SIRT2-Flag HeLa cells were lysed and immunopurified with anti-Flag agarose beads. The elution was subjected to SDS-PAGE and silver staining.
- B The bar graph shows the enrichment analysis of SIRT2-interacted proteins in the terms of GO biological process.
- C HeLa cell lysates were immunoprecipitated with control IgG, anti-G3BP1 (top), or anti-SIRT2 antibody (bottom), and then detected by immunoblotting.
- D MST assay analyzing the dissociation constant (Kd) of G3BP1 and SIRT2.
- E G3BP1-HA- and SIRT2-Flag-overexpressing cells were infected with HSV-1 (MOI = 0.5) for indicated times, and SIRT2-bound G3BP1 was immunoprecipitated and analyzed by immunoblotting.
- F Representative immunofluorescence staining of SIRT2 (red) and G3BP1 (green) in HSV-1 (MOI = 0.5, 4 h)-infected or untreated HeLa cells. Scale bars (bottom right), 10  $\mu\text{m}$ .
- G G3BP1-Flag plasmids were co-transfected with different amounts of HA-SIRT2 plasmids into HEK293T cells, and the acetylation level of G3BP1 was measured by immunoblotting.
- H G3BP1-Flag plasmids were co-transfected with WT or N168A-mutated HA-SIRT2 plasmids into HEK293T cells, and G3BP1 acetylation was detected by immunoblotting.
- I Hyperacetylated G3BP1 and SIRT2 proteins were immunopurified from HEK293T cells, respectively, and the *in vitro* deacetylation assay was performed as indicated.
- J The cell lysates of SIRT2 knocked-down HeLa cells were immunoprecipitated with anti-acetylysine agarose beads, and G3BP1 acetylation was detected by anti-G3BP1 antibody.
- K HEK293T cells were transfected with G3BP1-Flag plasmids and treated with AGK2 at indicated concentrations for 12 h, and the acetylation level of G3BP1 was detected by immunoblotting.

Source data are available online for this figure.



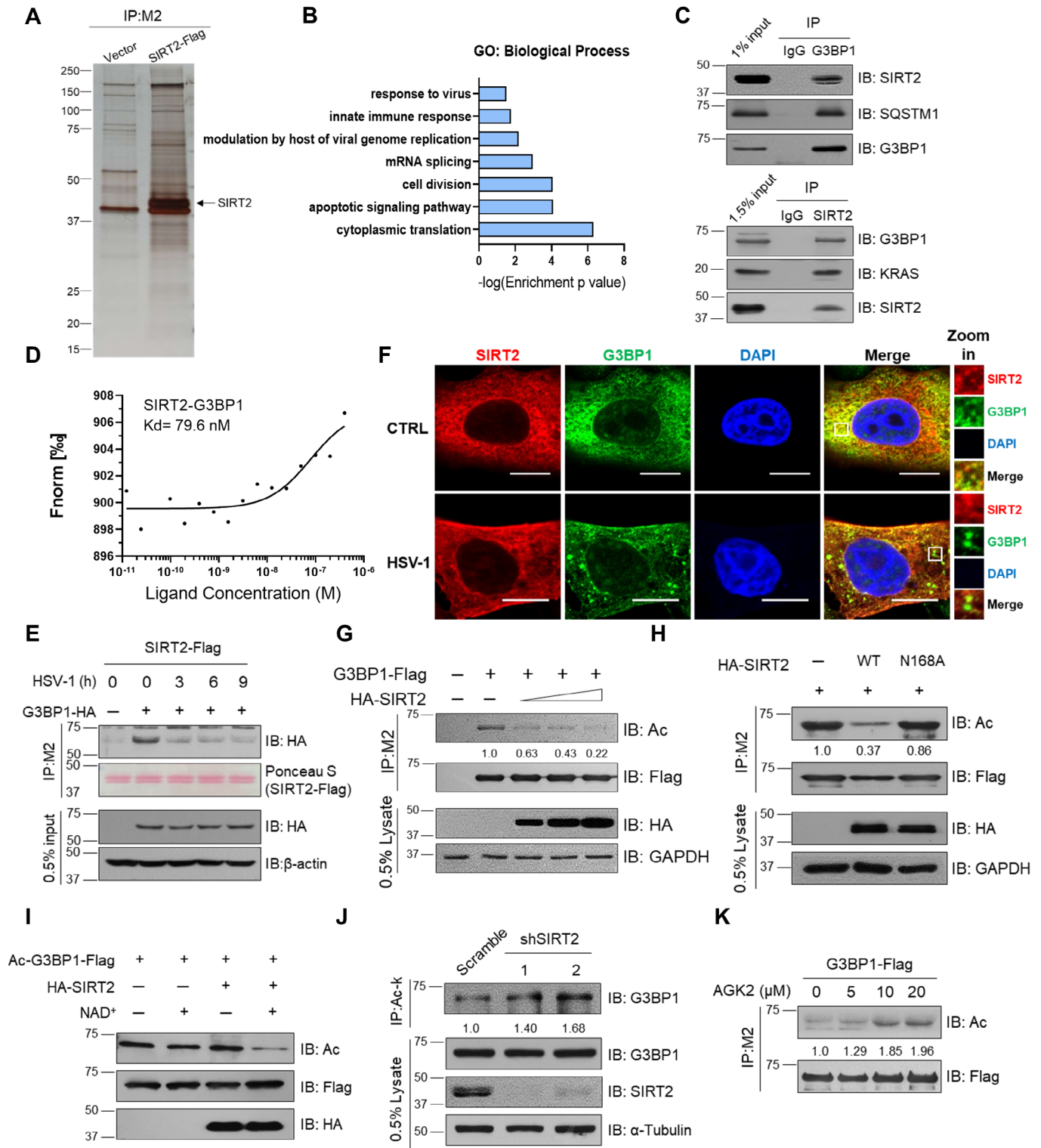


Figure 4.

promote the TNF $\alpha$  production (Fig EV5M), possibly because of the activation of TBK1-NF- $\kappa$ B-signaling pathway. Similar results were obtained by the qPCR analysis of IFN- $\beta$  and ISGs in the serum, liver,

and brain tissues from HSV-1-infected mice (Figs 7J and EV5N and O). Consistently, administration of RU.521 notably impaired the effects of AGK2 on promotion of the production of IFN- $\beta$  (Fig EV5P and Q).

Finally, we found that administration of AGK2 could prolong the survival time of the fatal infected mice (Fig 7K). However, the administration of anti-IFNAR1 antibodies in order to block the IFN pathway at the same time was capable of eliminating the protective effects of AGK2 (Figs 7L and EV5R). Taken together, AGK2 exhibited potential antiviral effect and protective role in the lethal HSV-1 infection mice models.

## Discussion

In this study, we find that SIRT2 is a unique regulator among the Sirtuin family, playing a negatively modulating cGAS-STING-signaling pathway. Upon DNA virus infection, SIRT2 expression levels decreased in a time-dependent manner, leading to increased production of IFN- $\beta$  and its downstream ISGs. The deficiency of

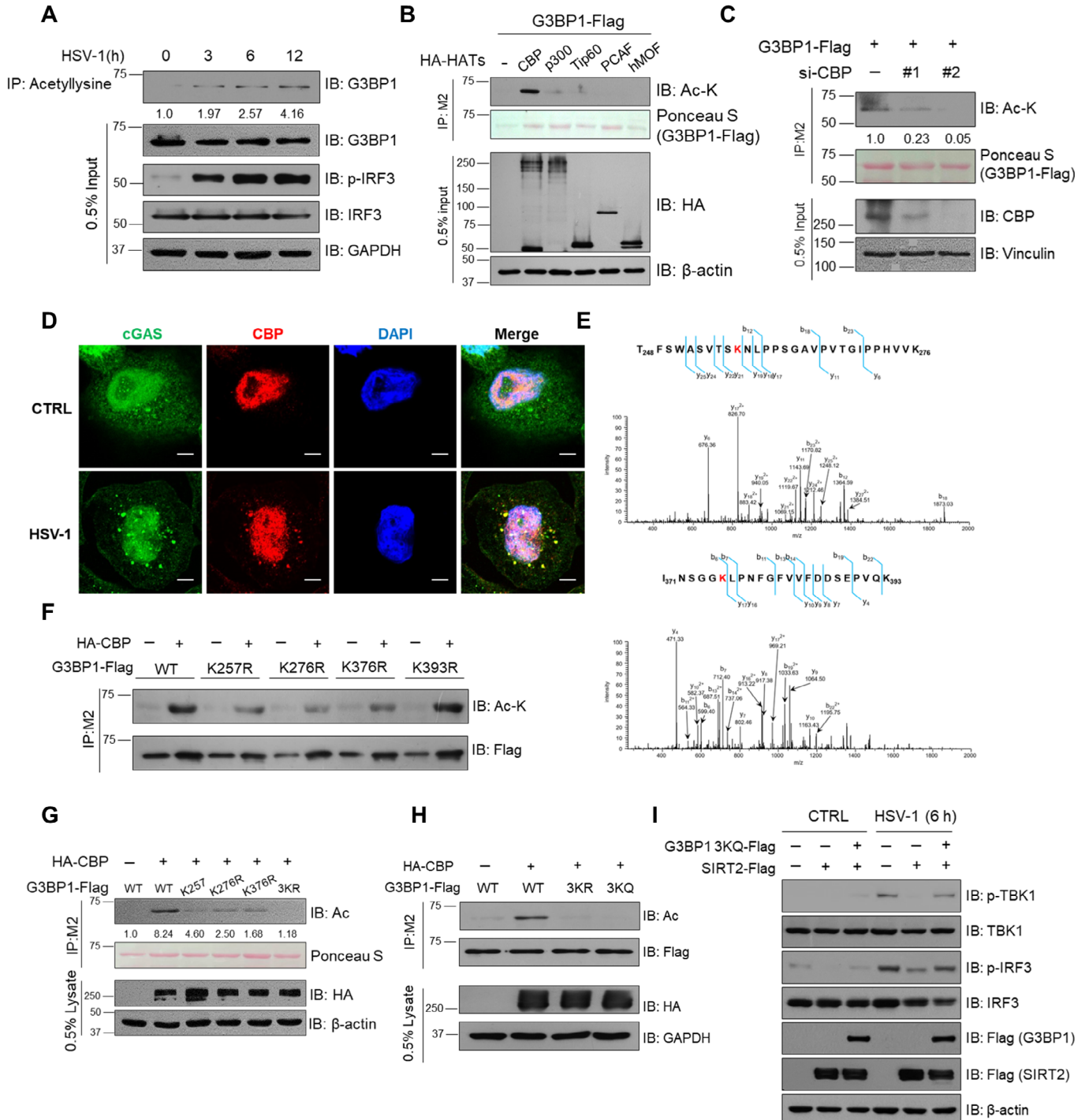


Figure 5.

**Figure 5. G3BP1 is acetylated by CBP in response to infection.**

- A HeLa cells were infected with HSV-1 (MOI = 0.5) for indicated time, and acetylated G3BP1 was immunoprecipitated by anti-acetylysine agarose beads.
- B HEK293T cells were transfected with plasmids as indicated, and G3BP1 acetylation was analyzed by immunoblot.
- C HEK293T cells were transfected with siRNAs against CBP along with G3BP1-Flag plasmids, and G3BP1 acetylation level was analyzed by immunoblotting.
- D Representative immunofluorescence staining of cGAS (green) and CBP (red) in HSV-1 (MOI = 1, 4 h)-infected HeLa cells. Scale bars (bottom right), 10  $\mu$ m.
- E G3BP1-Flag and CBP-HA plasmids were co-transfected into HEK293T cells to purify hyperacetylated G3BP1 proteins and subject to mass spectrometry analysis. The acetylated lysine residues were highlighted in red.
- F G3BP1-Flag WT and mutated plasmids were co-transfected with HA-CBP plasmids into HEK293T cells, and acetylation level of G3BP1 was analyzed by immunoblot.
- G HEK293T cells were transfected with plasmids as indicated, and G3BP1 proteins were immunoprecipitated and detected by anti-acetylysine antibody.
- H HEK293T cells were transfected with plasmids as indicated, and the acetylation level of G3BP1 WT, 3KR, or 3KQ was detected by immunoblot.
- I Immunoblot analysis of cGAS signaling in SIRT2-overexpressed and G3BP1 3KQ mutant-overexpressed HeLa cells infected with HSV-1 (MOI = 1) for 6 h.

Source data are available online for this figure.

SIRT2 promotes cGAS-DNA binding and droplet formation, which are crucial for cGAS activation. Further investigation revealed that SIRT2 regulation of the cGAS-STING-signaling pathway occurred through deacetylating G3BP1. Our findings suggest a potential antiviral strategy by modulating SIRT2.

SIRT2, as a unique cytoplasmic member of the Sirtuin family, has been previously linked to the pathogenesis, development, and prognosis of various diseases (Yang *et al*, 2020b). In our study, we discovered that SIRT2 expression levels were negatively modulated upon HSV-1 infection, with the up-regulation of HIF-1 $\alpha$ , at least partially, contributing to this process. AGK2, originally identified as a selected SIRT2 inhibitor for rescuing  $\alpha$ -synuclein toxicity and modified inclusion morphology in a cellular model of Parkinson's disease (Outeiro *et al*, 2007), has been found to inhibit hepatitis B virus replication (Yu *et al*, 2018) and alleviate lipopolysaccharide-induced neuroinflammation through regulation of mitogen-activated protein kinase phosphatase-1 (Jiao *et al*, 2020). Our discovery that AGK2 activates cGAS activity provides a novel antiviral strategy.

Post-translational modifications (PTMs) play a critical in protein stability, transportation, and activity, making them indispensable regulators of innate immunity (Liu *et al*, 2016). Acetylation, a reversible PTM mediated by acetyltransferases and deacetylases, has emerged as a crucial regulator in diverse cellular processes, including antipathogen response. Recent studies have highlighted the importance of acetylation in the regulation of key molecules involved in immunological processes, such as cGAS (Dai *et al*,

2019), retinoic acid-inducible gene-I (RIG-I) (Choi *et al*, 2016), and TBK1 (Tang *et al*, 2021). Our findings on SIRT2-regulating cGAS activation through G3BP1 demonstrated that cGAS activity could be regulated not only by acetylation on itself (Dai *et al*, 2019) but also by acetylation on G3BP1.

Innate immunity relies on pattern recognition receptors (PRRs) to detect invading microorganisms through germline-encoded pattern recognition receptors (PRRs) capable of sensing different pathogen-associated molecular patterns (PAMPs). cGAS, a recently discovered PRR, plays a central role in capturing cytoplasmic DNA and initiating downstream signaling, resulting in the production and secretion of type I interferon against pathogens. The precise regulation is critical for the activation of the cGAS-STING pathway, as it ensures a rapid antiviral response while preventing detrimentally excessive activation. Our study demonstrates that SIRT2 inhibits cGAS activation through direct interaction with and deacetylation of G3BP1, thereby adding another regulation mechanism for activation of the cGAS-STING pathway.

G3BP1, a central component of the stress granule assembly, is involved in a core protein-RNA interaction complex that forms in response to cellular stress (Guillén-Boixet *et al*, 2020). Stress granules assemble through liquid-liquid phase separation is driven by interactions distributed unevenly across the network. G3BP1 functions as a molecular switch that triggers RNA-dependent liquid-liquid phase separation in response to a rise of intracellular-free RNA concentrations (Yang *et al*, 2020a). G3BP1 also positively regulates

**Figure 6. G3BP1 acetylation inhibits cGAS activation.**

- A HeLa cells stably expressed G3BP1-Flag WT, 3KR, and 3KQ were lysed and immunoprecipitated with anti-Flag agarose beads. G3BP1-bound cGAS was analyzed by immunoblotting.
- B HeLa cells were transfected as indicated, and G3BP1-associated cGAS was analyzed by immunoblotting.
- C HeLa cells were transfected with G3BP1-Flag plasmids followed by AGK2 (10  $\mu$ M) treatment for 12 h, G3BP1-associated cGAS was immunoprecipitated and detected by immunoblotting.
- D qPCR analysis of Ifnb1 mRNA in G3BP1 knocked-out and G3BP1 WT, 3KR, or 3KQ rescued HeLa cells transfected with HT-DNA (2  $\mu$ g/ml, 6 h, left) or infected with HSV-1 (MOI = 1, 6 h, right) ( $n = 3$ , biological replicates).
- E Immunoblot analysis of cGAS signaling in G3BP1 knockout and rescued HeLa cells infected with HSV-1 (left) or transfected with HT-DNA (right).
- F ISD-bound cGAS was enriched by streptavidin magnetic beads from G3BP1 knockout and rescued HeLa cells, and analyzed by immunoblotting assay.
- G Representative immunofluorescence staining of G3BP1 (green) and cGAS (red) in HSV-1 (MOI = 1, 6 h)-infected HeLa rescued cells. Scale bars (bottom right), 10  $\mu$ m.
- H The percentage of cells stained with cGAS foci was quantified ( $n = 7$ , biological replicates).
- I Representative immunofluorescence staining of G3BP1 (green) and cGAS (red) in HSV-1-infected G3BP1 WT, 3KR, or 3KQ rescued HeLa cells. Scale bars (bottom right), 20  $\mu$ m.
- J The percentage of cells stained with cGAS foci was quantified, and at least 100 cells from each group were counted ( $n = 7$ , biological replicates).

Data information: \* $P < 0.05$ , \*\* $P < 0.01$ , \*\*\*\* $P < 0.0001$ . For panel (D), the two-tailed unpaired Student's  $t$ -test was used. For (H and J), the one-way ANOVA was used. Bars, mean  $\pm$  SD.

Source data are available online for this figure.

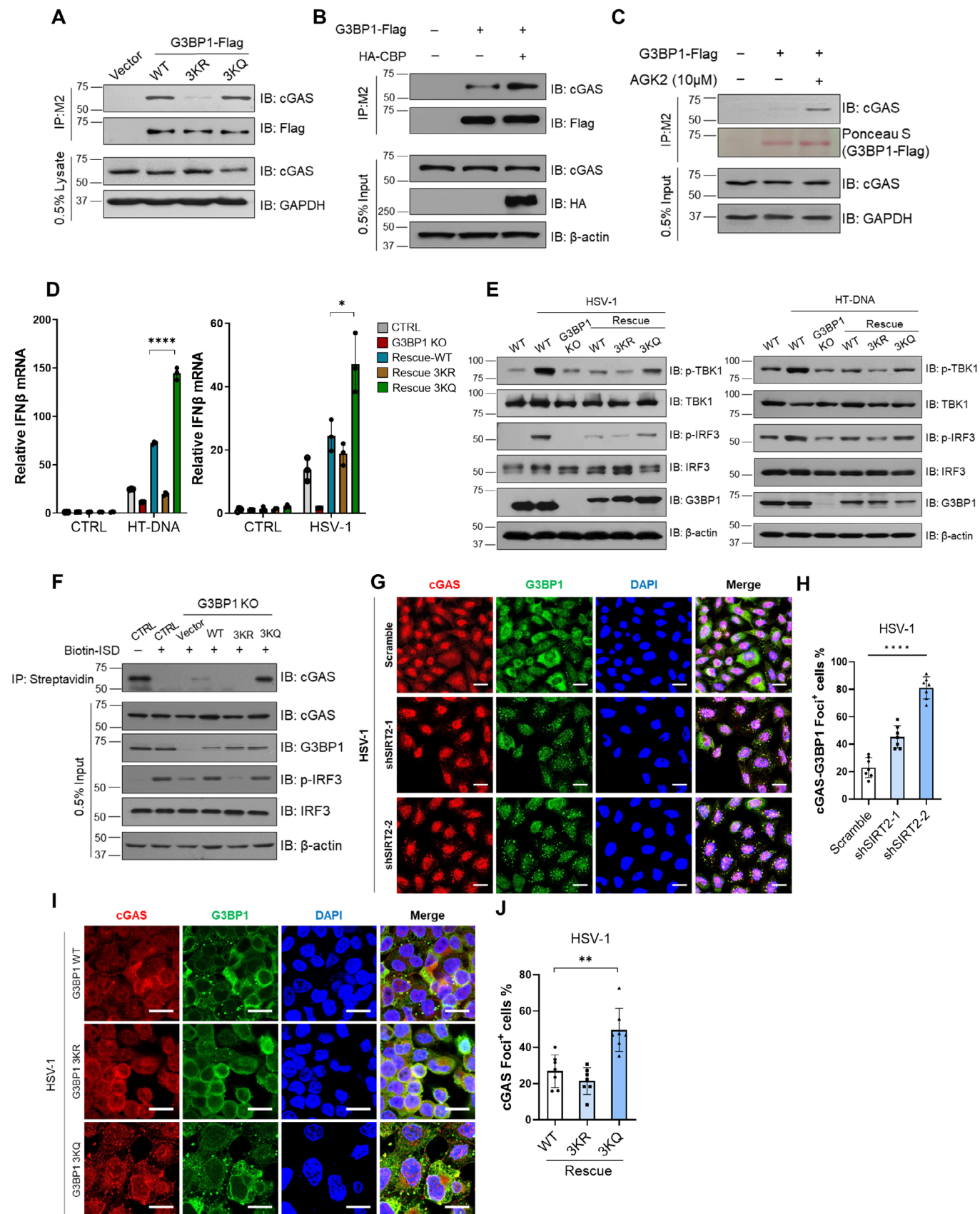


Figure 6.

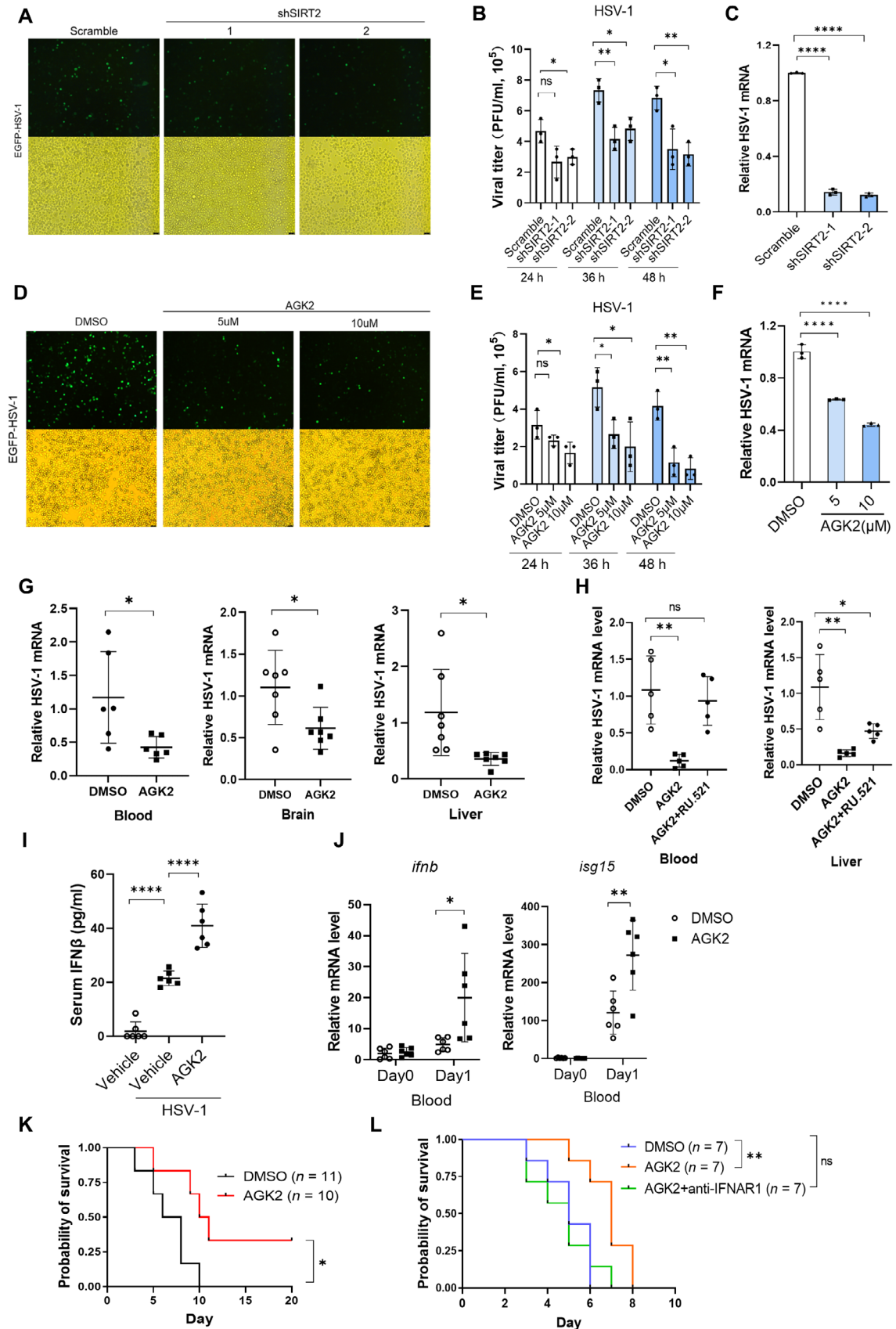


Figure 7.

**Figure 7. SIRT2 inhibition impairs HSV-1 replication *in vitro* and *in vivo*.**

- A SIRT2 knocked-down HeLa cells were infected with GFP-tagged HSV-1 (MOI = 0.5) for 12 h, and viral GFP expression was determined by fluorescence microscopy. Scale bars (bottom right), 50  $\mu$ m.
- B Plaque assay analysis of viral production by wild-type or shSIRT2 THP-1 cells infected with HSV-1 for indicated times ( $n = 3$ , biological replicates).
- C SIRT2 knocked-down THP-1 cells were infected with HSV-1 (MOI = 1) for 12 h, and HSV-1 mRNA (*LAT*) abundance was measured by qPCR analysis ( $n = 3$ , biological replicates).
- D HeLa cells were pretreated with AGK2 (10  $\mu$ M) for 12 h, followed by GFP-tagged HSV-1 (MOI = 0.5) infection for another 12 h. Viral GFP expression was determined by fluorescence microscopy. Scale bars (bottom right), 50  $\mu$ m.
- E Plaque assay analysis of viral production by AGK2 pre-treated or untreated THP-1 cells infected with HSV-1 for indicated times ( $n = 3$ , biological replicates).
- F AGK2 pretreated THP-1 cells were infected with HSV-1 (MOI = 1) for 12 h, and HSV-1 mRNA (*LAT*) abundance was measured by qPCR analysis ( $n = 3$ , biological replicates).
- G Age- and gender-matched C57BL/6 mice were pretreated with AGK2 (40 mg/kg) or DMSO 1 day before and 1 day after HSV-1 infection (PFU =  $5 \times 10^6$ ). Three days after infection, the serum, brain, and liver tissues were collected for qPCR analysis of HSV-1 RNA abundance ( $n = 6$ , biological replicates).
- H Age- and gender-matched C57BL/6 mice were administrated with AGK2 (40 mg/kg) alone, and AGK2 combined with RU.521 (5 mg/kg) or DMSO as described above. Three days after infection, tissues as indicated were retrieved for qPCR analysis of HSV-1 mRNA ( $n = 5$ , biological replicates).
- I Age- and gender-matched C57BL/6 mice were pretreated with AGK2 (40 mg/kg) or DMSO 1 day before and 1 day after HSV-1 infection (PFU =  $5 \times 10^6$ ). Three days after infection, serum IFN- $\beta$  concentration was analyzed by the ELISA ( $n = 6$ , biological replicates).
- J Age- and gender-matched C57BL/6 mice were pretreated with AGK2 (40 mg/kg) or vehicle 1 day before HSV-1 infection (PFU =  $5 \times 10^6$ ), and the serum of mice was retrieved on the next day for qPCR analysis of *ifnb1* and *isg15* ( $n = 6$ , biological replicates).
- K Survival analysis of age- and gender-matched C57BL/6 mice that were administrated with AGK2 (40 mg/kg) 1 day before, and 2 and 4 days after HSV-1 infection (PFU =  $10^7$ ). Log-rank (Mantel–Cox) test was used for statistical analysis ( $n = 11$  for DMSO,  $n = 10$  for AGK2).
- L Survival analysis of age- and gender-matched C57BL/6 mice that were administrated with AGK2 (40 mg/kg) alone or with AGK2 and anti-IFNAR1 (200  $\mu$ g per mouse) 1 day before and 2 days after HSV-1 infection (PFU =  $10^7$ ) ( $n = 7$ ).

Data information: NS, not significant, \* $P < 0.05$ , \*\* $P < 0.01$ , \*\*\* $P < 0.001$ , \*\*\*\* $P < 0.0001$ . For (B, E, G, and J), the two-tailed unpaired Student's *t*-test was used. For (C, F, H, and I), the one-way ANOVA was used. For (K and L), the Log-rank (Mantel–Cox) test was used. Bars, mean  $\pm$  SD. Source data are available online for this figure.

the activation of RIG-I pathway, via interacting with RIG-I, and increasing its expression levels by antagonizing RNF125, the E3 ligase of RIG-I (Yang *et al.*, 2019). It would be interesting to investigate whether G3BP1 acetylation and SIRT2 can also regulate these functions of G3BP1. Besides, a previous study indicated that histone deacetylase 6 (HDAC6) was able to de-acetylate G3BP1 at K376, promoting stress granules assembly (Gal *et al.*, 2019). HDAC6 was also found to be a putative component of stress granules (Kwon *et al.*, 2007). However, whether SIRT2-mediated G3BP1 deacetylation regulates antiviral responses through stress granules warrants further exploration.

While rapid production and secretion of type I IFN are essential for host defense against pathogens, excessive activation of the signaling pathway can lead to pathological effects such as autoimmunity. Systemic lupus erythematosus (SLE) and Aicardi–Goutieres

syndrome (AGS) are autoimmune diseases related to mutations in TREX1, a DNA exonuclease that can lead to the accumulated cytoplasmic DNA, which in turn activates cGAS (Stetson *et al.*, 2008; Gao *et al.*, 2015). In addition, SARS-CoV-2 infection has been reported to activate the cGAS-STING pathway through the release of mitochondrial DNA (mtDNA) in endothelial cells and macrophages, leading to cell death and type I IFN secretion. The sustained elevation of IFNs contributes to skin lesions and lung inflammation in COVID-19 patients (Di Domizio *et al.*, 2022). Thus, the regulation of SIRT2-mediated cGAS-STING inactivation could be potentially harnessed to reduce chronic inflammation or treat diseases related to SARS-CoV2.

In conclusion, our study provides valuable insights into the role of SIRT2 as a negative regulator of the cGAS-STING-signaling pathway and suggests targeting SIRT2 as antiviral strategies.

## Materials and Methods

### Reagents and Tools table

Reagent/Resource	Reference or source	Identifier or catalog number
<b>Experimental models</b>		
Human cell line: HEK293T	ATCC	Cat#CRL-11268
Human cell line: HeLa	ATCC	Cat#CCL-2
Human cell line: THP-1	ATCC	Cat#TIB-202
Mouse cell line: 4T1	ATCC	Cat#CRL-2539
Monkey cell line: Vero	ATCC	Cat#CCL-81
Mouse: C57BL/6	PKUHSC	N/A
TSurbo Chemically Competent Cell	Tsingke Biotechnology	Cat#TSC-C02
TSsetta Chemically Competent Cell	Tsingke Biotechnology	Cat#TSC-E04
HSV-1 (Herpes Simplex Virus 1, 17 strain)	Zhengfan J. (Peking University)	N/A

Reagents and Tools table (continued)

Reagent/Resource	Reference or source	Identifier or catalog number
VSV (Indiana strain)	J. Rose (Yale University)	N/A
HSV-1-GFP (Herpes Simplex Virus 1-GFP, Kos strain)	Zhengfan J. (Peking University)	N/A
<b>Recombinant DNA</b>		
pQCXIH- G3BP1-Flag	This manuscript	N/A
pQCXIH- G3BP1-Flag 3KR	This manuscript	N/A
pQCXIH- G3BP1-Flag 3KQ	This manuscript	N/A
pcDNA3.1-G3BP1-Flag	This manuscript	N/A
pcDNA3.1-G3BP1-Flag K257R	This manuscript	N/A
pcDNA3.1-G3BP1-Flag K276R	This manuscript	N/A
pcDNA3.1-G3BP1-Flag K376R	This manuscript	N/A
pcDNA3.1-G3BP1-Flag K393R	This manuscript	N/A
pcDNA3.1-G3BP1-Flag 3KR	This manuscript	N/A
pcDNA3.1-G3BP1-Flag 3KQ	This manuscript	N/A
pcDNA3.1-HA-SIRT2	This manuscript	N/A
pcDNA3.1-HA-SIRT2 N168A	This manuscript	N/A
pcDNA3.1-HA-HATs (CBP, p300, PCAF, TIP60, and hMOF)	This manuscript	N/A
pHBLV-SIRT2-Flag	This manuscript	N/A
pHBLV-G3BP1-Flag	This manuscript	N/A
pHBLV-G3BP1-Flag 3KR	This manuscript	N/A
pHBLV-G3BP1-Flag 3KQ	This manuscript	N/A
pLKO.1-puro-shRNA-SIRT2	This manuscript	N/A
LentiCRISPRv2-G3BP1	This manuscript	N/A
<b>Antibodies</b>		
Mouse anti-G3BP1	Santa Cruz Biotechnology	Cat#sc-365338; RRID: AB_10846950
Mouse anti-cGAS	Santa Cruz Biotechnology	Cat#sc-515777; RRID: AB_2734736
Mouse anti- $\beta$ -actin	Santa Cruz Biotechnology	Cat#sc-8432; RRID: AB_626630
Mouse anti- $\alpha$ -tubulin	Santa Cruz Biotechnology	Cat#sc-8035; RRID: AB_628408
Mouse anti-CBP	Santa Cruz Biotechnology	Cat#sc-7300; RRID: AB_626817
Mouse anti-Vinculin	Santa Cruz Biotechnology	Cat#sc-73614; RRID: AB_1131294
Mouse anti-SIRT1	Santa Cruz Biotechnology	Cat# sc-74465; RRID: AB_1129462
Rabbit anti- phospho-IRF3 (Ser386)	Abcam	Cat#ab76493; RRID: AB_1523836
Rabbit anti-IRF3	Abcam	Cat#ab68481; RRID: AB_11155653
Rabbit anti-TBK1	Abcam	Cat#ab40676; RRID: AB_776632
Rabbit anti-SIRT1	Abcam	Cat#ab189494; RRID: AB_2864311
Rabbit anti-SIRT2	Abcam	Cat#ab134171; RRID: AB_2716787
Rabbit anti-GAPDH	Cell Signaling Technology	Cat#5174; RRID: AB_10622025
Rabbit anti-cGAS	Cell Signaling Technology	Cat#15102; AB_2732795
Rabbit anti- phospho-TBK1 (Ser172)	Cell Signaling Technology	Cat#5483; RRID: AB_10693472
Rabbit anti-acetylated-Lysine	Cell Signaling Technology	Cat#9441; RRID: AB_331805
Rabbit anti-CBP	Cell Signaling Technology	Cat#7389; RRID: AB_2616020

Reagents and Tools table (continued)

Reagent/Resource	Reference or source	Identifier or catalog number
Rabbit anti-SIRT3	Cell Signaling Technology	Cat#2627; RRID: AB_2188622
Rabbit anti-SIRT5	Cell Signaling Technology	Cat#8782; RRID: AB_2716763
Rabbit anti-SIRT6	Cell Signaling Technology	Cat#12486; RRID: AB_2636969
Rabbit anti-SIRT7	Cell Signaling Technology	Cat#5360; RRID: AB_2716764
Rabbit anti-Caspase-3	Cell Signaling Technology	Cat#14220; RRID: AB_2798429
Rabbit anti-HIF-1 $\alpha$	Cell Signaling Technology	Cat#36169; RRID: AB_2799095
Mouse anti-Flag	Sigma-Aldrich	Cat#F-3165; RRID: AB_259529
Rabbit anti-SIRT4	Sigma-Aldrich	Cat#HPA029691; RRID: AB_10600118
Rabbit anti-LC3B	Sigma-Aldrich	Cat#L7543; RRID: AB_796155
Mouse anti-HA	Thermo Fisher Scientific	Cat#26183; RRID: AB_2533052
Rabbit anti-Herpes Simplex Virus Type 1	Thermo Fisher Scientific	Cat#PA5-103293; RRID: AB_2815975
Donkey anti-rabbit Alexa Fluor 488	Thermo Fisher Scientific	Cat#A21206; RRID: AB_2535792
Donkey anti-mouse Alexa Fluor 594	Thermo Fisher Scientific	Cat#A-21203; RRID: AB_141633
Rabbit anti-cGAS	Proteintech	Cat#26416-1-AP; RRID: AB_2880507
Rabbit anti-SQSTM1/p62	Proteintech	Cat#18420-1-AP; RRID: AB_10694431
Rabbit anti-G3BP1	Proteintech	Cat#13057-2-AP; RRID: AB_2232034
<b>Oligonucleotides and other sequence-based reagents</b>		
Human SIRT1 siRNA: GGCUGAUGGUAAUCAGUATT	Tsingke Biotechnology	N/A
Human SIRT2 siRNA: UGCUCAUCAACAAGGAGAATT	Tsingke Biotechnology	N/A
Human SIRT3 siRNA: CAACGUCACUCACUACUUUTT	Tsingke Biotechnology	N/A
Human SIRT4 siRNA: CGAUUGCAAUACUGAACAUUTT	Tsingke Biotechnology	N/A
Human SIRT5 siRNA: CGUCCACACGAAACCAGAUUTT	Tsingke Biotechnology	N/A
Human SIRT6 siRNA: GAAUGUGCCAAGUGUAAGATT	Tsingke Biotechnology	N/A
Human SIRT7 siRNA: GGGAGUACGUGCGGGUGUUTT	Tsingke Biotechnology	N/A
Human CBP siRNA-1: UAUCAAGAAUAGGUUAUUAUUTT	Tsingke Biotechnology	N/A
Human CBP siRNA-2: GUUUACAUAACAAGGCAUUTT	Tsingke Biotechnology	N/A
Human HIF-1 $\alpha$ siRNA: GAUGAAAGAAUUAACCGAAUUTT	Tsingke Biotechnology	N/A
Human SIRT2 shRNA-1: 5'-CCGGTATGACAACCTAGAGAAGTACCTCGAGGTACTTCTAGGTTGTACATTTTTTG-3'	Tsingke Biotechnology	N/A
Human SIRT2 shRNA-2: 5'-CCGGCAGCGCGTTTCTTCTCCTGACTCGAGTACAGGAGAAGAACGCGCTGTTTTTG-3'	Tsingke Biotechnology	N/A
Human G3BP1 sgRNA: CACCGAACGTTTGTCTTGTCTCTCTG	Tsingke Biotechnology	N/A
Human IFNB qPCR primer: F: AGGACAGGATGAACCTTTGAC R: TGATAGACATTAGCCAGGAG	Tsingke Biotechnology	N/A
Human ISG15 qPCR primer: F: CGCAGATACCCAGAAGATCG R: TTCGTGCGATTGTCCACCA	Tsingke Biotechnology	N/A
Human IFIT1 qPCR primer: F: GCGCTGGGTATGCGATCTC R: CAGCCTGCCTTAGGGGAAG	Tsingke Biotechnology	N/A
Human IFI27 qPCR primer: F: TGCTCTCACCTCATCAGCAGT R: CACAACCTCCAATCACAAC	Tsingke Biotechnology	N/A
Human SIRT1 qPCR primer:	Tsingke Biotechnology	N/A



Reagents and Tools table (continued)

Reagent/Resource	Reference or source	Identifier or catalog number
F: TAGACACGCTGGAACAGGTTGC R: CTCCTCGTACAGCTTCACAGTC		
Human SIRT2 qPCR primer: F: CTGCGGAACTTATTCTCCAGAC R: CCACCAACAGATGACTCTGCG	Tsingke Biotechnology	N/A
Human SIRT3 qPCR primer: F: CCCTGGAACTACAAGCCCAAC R: GCAGAGGCAAGGTTCCATGAG	Tsingke Biotechnology	N/A
Human SIRT4 qPCR primer: F: GTGGATGCTTTGCACACCAAGG R: GGTTCAGGACTTGGAAACGCTC	Tsingke Biotechnology	N/A
Human SIRT5 qPCR primer: F: GTCCACACGAAACCAGATTTGCC R: TCCTCTGAAGGTCGGAACACCA	Tsingke Biotechnology	N/A
Human SIRT6 qPCR primer: F: TGGCAGTCTTCCAGTGTTGGT R: CGCTCTCAAAGGTGGTGTGCGAA	Tsingke Biotechnology	N/A
Human SIRT7 qPCR primer: F: TGGAGTGTGGACACTGCTTCAG R: CCGTCACAGTTCTGAGACACCA	Tsingke Biotechnology	N/A
Human GAPDH qPCR primer: F: GACTCAACGGATTTGGTCTG R: TTGATTTTGGAGGGATCTCG	Tsingke Biotechnology	N/A
Mouse Ifnb qPCR primer: F: TCCGAGCAGAGATCTTCAGGAA R: TGCAACCACCACTCATTCTGAG	Tsingke Biotechnology	N/A
Mouse Isg15 qPCR primer: F: TGA CTGTGAGAGCAAGCAGC R: CCCAGCATCTTCACCTTTA	Tsingke Biotechnology	N/A
Mouse Ifi27 qPCR primer: F: GCAGTCTCTGGCACCATTCTAG R: ATGGTGCCAACTTCAGTGCTC	Tsingke Biotechnology	N/A
Mouse Gapdh qPCR primer: F: CATCACTGCCACCCAGAAGACTG R: ATGCCAGTGAGCTTCCCGTTCAG	Tsingke Biotechnology	N/A
HSV-1 qPCR primer: F: TGGGACACATGCCTTCTTGG R: ACCCTTAGTCAGACTCTGTTACTTACCC	Tsingke Biotechnology	N/A
ISD: 5'-TACAGATCTACTAGTGATCTATG-3'	Tsingke Biotechnology	N/A
<b>Chemicals, enzymes and other reagents</b>		
CoCl <sub>2</sub>	Sigma-Aldrich	Cat#C8661
Nicotinamide	Sigma-Aldrich	Cat#N9910
Puromycin	Sigma-Aldrich	Cat#P8833
DAPI	Sigma-Aldrich	Cat#D9542
Anti-HA agarose beads	Sigma-Aldrich	Cat#E6779
Anti-Flag agarose beads	Sigma-Aldrich	Cat#A2220
HT-DNA	Sigma-Aldrich	Cat#D6898
Flag-peptide	Sigma-Aldrich	Cat#F3290
PMA	Sigma-Aldrich	Cat#P8139
Hygromycin B	Thermo Fisher Scientific	Cat#10687010
Lipofectamine RNAiMAX	Thermo Fisher Scientific	Cat#13778075
Streptavidin Magnetic Beads	Thermo Fisher Scientific	Cat#88816
Lipofectamine 2000	Thermo Fisher Scientific	Cat#11668027

Reagents and Tools table (continued)

Reagent/Resource	Reference or source	Identifier or catalog number
Protein A/G agarose beads	Thermo Fisher Scientific	Cat#20241
2'3'-cGAMP	Abcam	Cat#ab144865
AGK2	Selleck	Cat#S7577
Anti-mouse IFNAR-1-InVivo	Selleck	Cat#DD230407-0128
Anti-acetyl lysine agarose beads	Immunechem	Cat#ICP0388
Human IFN- $\beta$	Peptotech	Cat#300-02BC
RU.521	MedChemExpress	Cat#HY-114180
6xHis-tagged cGAS protein	MedChemExpress	Cat#HY-P72337
BSA	Beyotime	Cat#P0007
Flag peptides	Beyotime	Cat#P9801
HA peptides	Beyotime	Cat#P9808
4% paraformaldehyde	Biosharp	Cat#BL539A
<b>Software</b>		
GraphPad Prism 8.0	<a href="https://www.graphpad.com">https://www.graphpad.com</a>	N/A
NIH ImageJ	<a href="https://imagej.nih.gov/ij/">https://imagej.nih.gov/ij/</a>	N/A
Toppgene	<a href="https://toppgene.cchmc.org/">https://toppgene.cchmc.org/</a>	N/A
ZEN 3.2	<a href="https://www.zeiss.com">https://www.zeiss.com</a>	N/A
<b>Other</b>		
KOD Plus Mutagenesis Kit	TOYOBO	Cat#SMK-101B
Dual-Luciferase Reporter Assay	Promega	Cat#E1910
First Strand cDNA Synthesis kit	Yeasen	Cat#11123ES10
Mouse Interferon $\beta$ ELISA Kit	CUSABIO	Cat#CSB-E04945m
Mouse Tumor necrosis factor $\alpha$ ELISA Kit	CUSABIO	Cat#CSB-E04741m

## Methods and Protocols

### Mice

All animals care and use adhered to the Guide for the Care and Use of Laboratory Animals of the Chinese Association for Laboratory Animal Science, and mice were housed under 12/12-h light/dark cycle. All procedures of animal handling were approved by the Animal Care Committee of Peking University Health Science Center (permit number LA 2016240).

C57BL/6 mice (male, 4–6 weeks old) were purchased from the Department of Laboratory Animal Science of Peking University Health Science Center, Beijing. Mice were given AGK2 (40 mg/kg) via intraperitoneal injection 1 day before virus infection, and 1 and 3 days after infection. Mice were infected with  $5 \times 10^6$  plaque-forming units (PFU) of HSV-1 per mouse via intravenous injection for qPCR and ELISA analyses. For survival analysis, mice were infected with  $5 \times 10^7$  PFU of HSV-1 per mouse.

### Cell culture, transfection, infection, and treatment

HEK293T, HeLa, Vero, THP-1, and 4T1 cells were obtained from American Type Culture Collection (ATCC). HEK293T, HeLa, and Vero cells were cultured in Dulbecco's modified Eagle's medium

(DMEM) supplemented with 10% fetal bovine serum (FBS), 100 U/ml penicillin, and 100  $\mu$ g/ml streptomycin. THP-1 and 4T1 were cultured in RPMI-1640 supplemented with 10% fetal bovine serum (FBS), 100 U/ml penicillin, and 100  $\mu$ g/ml streptomycin. All cells were negative for mycoplasma contamination. THP-1 cells were differentiated with PMA (0.1  $\mu$ M) for around 24 h before transfection or virus infection.

Interferon stimulatory DNA or HT-DNA was transfected via Lipofectamine 2000 (Thermo Fisher Scientific) at a final concentration of 2  $\mu$ g/ml. siRNAs were transfected via Lipofectamine RNAiMAX (Thermo Fisher Scientific) according to the manufacturer's instructions. The siRNAs used in this manuscript are shown in the Reagents and Tools table.

Herpes simplex virus-1 (17 strain) and VSV (Indiana strain) were used for cell infection. The MOI of virus and infection time are indicated in legends of every panel.

For cGAMP stimulation, THP-1 cells were incubated with cGAMP (1  $\mu$ g/ml) for 45 min at 37°C in the permeabilization buffer (50 mM HEPES, pH 7; 100 mM KCl; 3 mM MgCl<sub>2</sub>; 0.1 mM DTT; 85 mM sucrose; 0.2% BSA; 1 mM ATP; and 0.1 mM GTP) supplemented with 1  $\mu$ g/ml digitonin (D141, Sigma-Aldrich). Cells were then cultured in RPMI-1640 medium for another 4 h.

### Luciferase assay and type I IFN bioassay

HEK293T or HeLa cells were seeded on 6-well plate and transfected with 500 ng of the IFN $\beta$ -luciferase reporter plasmid, 500 ng pRL-TK, and equal amount of various expression plasmids or empty control plasmids. Twenty-four hours later, with or without virus infection for another 12 h, the reporter gene activity was measured via the Dual-Luciferase Reporter Assay System (E1910, Promega) and normalized by Renilla luciferase activity.

Type I IFNs in THP-1 culture medium were measured with 2fTGH-ISRE cell line stably expressing an ISRE-Luciferase reporter. After being infected with HSV-1 for 24 h, 1 ml THP-1 culture medium was incubated with 2fGTH-ISRE-Luciferase cells (Cao *et al*, 2019) and seeded in 12-well plate for 6 h. Cells were lysed in passive lysis buffer and subjected to luciferase quantification kit (E1910, Promega).

### shRNA knockdown and CRISPR-Cas9 system

To generate SIRT2 knockdown cell lines, 21 bp short hairpin RNA (shRNA) sequences were ligated into pLKO.1 (Sigma-Aldrich) plasmid and then co-transfected with viral packaging plasmids (psPAX2 and pMD2.G) into HEK293T cells. Forty-eight hours after transfection, the culture medium was collected and filtered through a 0.22  $\mu$ m strainer. HeLa or THP-1 cells were infected with the viral supernatant for 48 h and then selected with 1 mg/ml puromycin for 1 week.

To generate G3BP1 knockout cell lines, the sgRNA sequences were ligated into LentiCRISPRv2 plasmid and then co-transfected with viral packaging plasmids (psPAX2 and pMD2.G) into HEK293T cells. Forty-eight hours after transfection, the culture medium was collected and filtered through a 0.22  $\mu$ m strainer. HeLa cells were infected with viral supernatant for 48 h and then selected with 1  $\mu$ g/ml puromycin for 2 weeks.

### Stably expressed and rescued cell lines

To generate SIRT2-Flag or G3BP1-Flag stably overexpressed cell lines, cDNA of SIRT2, wild-type, and mutated G3BP1 were cloned into pHBLV vector (Hanbio), and the plasmid was co-transfected with viral packaging plasmids (psPAX2 and pMD2.G) into HEK293T cells for 48 h to obtain the supernatants. HeLa cells were further infected with the viral supernatants for 48 h and selected with 1  $\mu$ g/ml puromycin for 1 week.

To generate G3BP1-Flag rescued cell lines, cDNA of wild-type and mutated G3BP1 was subcloned into pQCXIH vector. The plasmid was co-transfected with viral packaging plasmids into HEK293T cells. The viral supernatants were further infected into G3BP1 KO HeLa cells. The infected cells were selected by 150  $\mu$ g/ml hygromycin for 2 weeks.

### Co-immunoprecipitation and protein purification

Harvested cells were lysed in Flag lysis buffer [50 mmol/l Tris-HCl (pH 7.9), 137 mmol/l NaCl, 1% Triton X-100, 0.2% Sarkosyl, 1 mmol/l NaF, 1 mmol/l Na<sub>3</sub>VO<sub>4</sub>, and 10% glycerol] containing protease inhibitor cocktail (Selleck), 1 mmol/l dithiothreitol, and 1 mmol/l phenylmethyl sulfonyl fluoride. The supernatants were incubated with anti-Flag, anti-HA agarose beads, or streptavidin magnetic beads at 4°C overnight, or incubated with anti-SIRT2 (sc-28298, Santa Cruz) at 4°C overnight and further with protein A/G agarose beads for another 2 h at 4°C. After being washed with lysis

buffer five times, proteins were eluted via boiling with 1  $\times$  loading buffer and then analyzed by western blotting. For elution of the streptavidin magnetic beads, the extra biotin (4 mg/ml) was added to the loading buffer.

GST-G3BP1 was expressed from Rosetta bacterial cells and purified by the GST agarose (Novagen). After incubation, beads were eluted by GSH and diluted by four volumes of BC100 buffer rapidly. HA-SIRT2 and G3BP1-Flag were purified from HEK293T cells, enriched by HA and Flag agarose beads, and eluted by HA and Flag peptides, respectively.

### cGAMP quantification

For 2'3'-cGAMP measurement, the commercial ELISA kit based on the competition between 2'3'-cGAMP and 2'3'-cGAMP-HRP was used (501700, Cayman) (Su *et al*, 2020). Briefly, 10<sup>6</sup> THP-1 or HeLa cells were seeded into six-well plates, and THP-1 cells were differentiated with PMA as described above. After transfected with HT-DNA (2  $\mu$ g/ml) for 3 h, cells were harvested and lysed with the protein extraction reagent (78503, Thermo Fisher Scientific). After centrifuging for 15 min, the supernatant was collected for cGAMP quantification according to the manufacturer's instructions. The protein concentration was analyzed through Bradford protein assay kit (5000201, BIO-RAD) for normalization.

### Immunofluorescence staining

Cells were seeded into glass coverslips in six-well plates and washed with warm PBS three times. Cells were fixed with 4% paraformaldehyde (PFA) in PBS for 20 min and then permeabilized with 0.3% Triton X-100 in PBS for 20 min at room temperature (RT). After rinsing with washing buffer (0.1% Triton X-100 in PBS) three times, the cells were blocked for 2 h at RT with blocking buffer (5% BSA, 5% goat serum, and 1% Na<sub>2</sub>S<sub>2</sub>O<sub>8</sub> in washing buffer) and then incubated with antibodies at 4°C overnight. Next, cells were incubated with the secondary antibodies conjugated with Alexa-488 or Alexa-594 at room temperature for 2 h, followed by incubated with DAPI in PBS for 10 min. Images were visualized with a confocal microscope (Zeiss LSM880). cGAS droplets and cell numbers were quantified using ImageJ software and the Analyze Particles function, with a minimum size requirement of 200 pixels<sup>2</sup>.

### Mass spectrometry for identification of SIRT2 interactors

SIRT2-Flag stably expressed HeLa cells and wild-type HeLa cells were separately seeded into 10 cm dishes, and when at 80% confluence cells were harvested and lysed in Flag lysis buffer [50 mmol/l Tris-HCl (pH 7.9), 137 mmol/l NaCl, 1% Triton X-100, 0.2% Sarkosyl, 1 mmol/l NaF, 1 mmol/l Na<sub>3</sub>VO<sub>4</sub>, and 10% glycerol] containing protease inhibitor cocktail, 1 mmol/l dithiothreitol, and 1 mmol/l phenylmethyl sulfonyl fluoride. Anti-Flag M2 agarose (A2220, Sigma) was mixed with equal number of total proteins (3,500  $\mu$ g) overnight. Eluted SIRT2-associated proteins were detected by semi-quantitative LC-MS/MS (Q Exactive HF, Peking University Medical and Health Analysis Center), and proteins detected in wild-type HeLa cells were subtracted.

### RNA isolation and quantitative PCR

Total RNA was extracted with TRI reagent (93289, Sigma-Aldrich). One microgram RNA was reverse transcribed into cDNA via a cDNA synthesis kit (11141ES60, Yeasen). Quantitative PCR was performed

in 7500 Fast Real-time PCR System (Applied Biosystems) with qPCR SYBR Green Master Mix (11202ES03, Yeasen). Human GAPDH and mouse gapdh were used for normalization. The sequence information of primers used in this work is shown in [Reagents and Tools table](#).

#### **In vitro phase condensation assay**

The analysis of cGAS condensation *in vitro* was performed as previously described (Zhao *et al*, 2022). cGAS was from MedChemExpress, while G3BP1 was purified from HEK293T cells as described above. FAM-conjugated ISD was synthesized at Tsingke Biotechnology and annealed as described above. cGAS and G3BP1 were diluted with PBS, respectively. After incubating with ISD, the mixture was added into a glass-bottom cell culture dish and observed via the confocal microscope (Zeiss LSM880).

#### **Microscale thermophoresis analysis**

The binding affinity between SIRT2 and G3BP1 was measured by NanoTemper Monolith NT.115 instrument (NanoTemper Technologies, Germany). Flag-tagged G3BP1 was purified from HEK293T cells via M2 agarose beads and Flag peptides. 6xHis-tagged SIRT2 was from Cloud clone (RPA430Hu01). 6xHis-SIRT2 was firstly labeled using His-tag labeling kit at room temperature for 30 min, and then diluted with binding buffer (50 mM Tri-HCl, pH 7.5, 10 mM KCl, 5 mM MgCl<sub>2</sub>, and 0.005% Tween 20) to ensure the fluorescence intensity during the analysis was about 500 RU. In this assay, the final concentration of SIRT2 was 100 nM. G3BP1 was serially diluted in the binding buffer (16 points, 1:2 dilutions, and started at 500 μM), and then mixed and incubated with an equal volume of the diluted SIRT2 at room temperature for 5 min. After incubation, the mixture was loaded into the premium-treated capillaries and measured in NanoTemper Monolith NT.115 Instrument (NanoTemper Technologies, Germany). The KD values were fitted by NanoTemper Monolith affinity software (NanoTemper Technologies, Germany) using 1:1 binding mode.

#### **Plaque assay**

Viral titers from the cell culture medium were analyzed by plaque-forming assay, as previously described (Cao *et al*, 2019). Briefly, virus containing medium of HSV-1- or VSV-infected THP-1 cells was collected and serially diluted, which was then added to the confluent Vero cells. After 1 h of incubation, supernatants were removed, cells were washed with PBS, and culture medium containing 2% (w/v) methylcellulose was overlaid for 24 h. Then, cells were fixed with 4% paraformaldehyde and then stained with crystal violet. The plaques were counted, and average counts were multiplied by the dilution factor to determine the viral titer as PFU per milliliter.

#### **Cell viability assay**

Wild-type and SIRT2 knockdown HeLa or THP-1 cells were seeded in 96-well plates at 10<sup>4</sup> cells per well and grew overnight. THP-1 cells were differentiated with PMA (0.1 μM) 24 h before test. After being infected with HSV-1 for indicated time, the cell viability assay was performed using Cell Counting Kit-8 (CCK8) (Dojindo), according to the manufacturer's instruction.

#### **ELISA**

Mice were infected with 5 × 10<sup>6</sup> plaque-forming units (PFU) of HSV-1 per mouse via intravenous injection, and given AGK2

(40 mg/kg) or vehicle via intraperitoneal injection 1 day before and 1 day after virus infection. Three days post-infection, the secreted IFN-β and TNF-α in the serum were analyzed with ELISA kits according to the manufacturer's instruction.

#### **In vitro deacetylation assay**

HA-SIRT2 was purified from HEK293T cells while the hyperacetylated Flag-G3BP1 was purified from HEK293T cells co-transfected with CBP. The reaction mixture contained 10 × Ac buffer (200 mM pH 8.0 HEPES, 10 mM DTT, 10 mM PMSF, and 1 mg/ml BSA), 2 × De-Ac buffer (8 mM MgCl<sub>2</sub>, 100 mM NaCl and 20% glycerol), and hyperacetylated G3BP1. SIRT2 and NAD<sup>+</sup> (1 mM) were present or absent as indicated. The reaction mixture was incubated at 37°C for 2 h and then boiled in the SDS sample buffer.

#### **Statistical analyses**

The experiments were performed three times independently and the repeated experiments showed similar results. The experiments are not blinded to researchers. Statistical analyses between two groups were performed with a two-tailed unpaired Student's *t*-test, and analysis of multiple comparisons was performed with one-way ANOVA. The Log-rank (Mantel-Cox) test was performed for the survival analysis. All statistical analyses were examined using GraphPad prism 9.0. Data were presented as mean ± standard deviation (S.D.). A difference was considered statistically significant at a value of *P* < 0.05. \**P* < 0.05, \*\**P* < 0.01, \*\*\**P* < 0.001, and \*\*\*\**P* < 0.0001, which were considered statistically significant.

## **Data availability**

Data are available via ProteomeXchange with identifier PXD045456 (<http://www.ebi.ac.uk/pride/archive/projects/PXD045456>).

**Expanded View** for this article is available [online](#).

#### **Acknowledgements**

We thank Zhengfan Jiang (Peking University) for providing us with cGAS plasmid and HSV-1 viruses; and Xiaoyun Liu (Peking University) for the assistance with mass spectrometry analysis. We thank the core facility at Peking University Health Science Center for experimental help. JL was supported by grants from the National Natural Science Foundation of China (82172959, 81874147, and 81671389).

#### **Author contributions**

**Yutong Li:** Formal analysis; validation; investigation; visualization; methodology; writing – original draft. **Juntao Bie:** Formal analysis; validation; investigation; visualization; methodology. **Chen Song:** Formal analysis; validation; investigation; methodology. **Yunfei Li:** Resources; methodology. **Tianzhuo Zhang:** Formal analysis; validation; investigation; methodology. **Haishuang Li:** Resources; methodology. **Long Zhao:** Resources; methodology. **Fuping You:** Conceptualization; supervision; project administration; writing – review and editing. **Jianyuan Luo:** Conceptualization; supervision; funding acquisition; visualization; project administration; writing – review and editing.

#### **Disclosure and competing interests statement**

The authors declare that they have no conflict of interest.

## References

- Akira S, Uematsu S, Takeuchi O (2006) Pathogen recognition and innate immunity. *Cell* 124: 783–801
- Anisimov S, Takahashi M, Kakahana T, Katsuragi Y, Kitaura H, Zhang L, Kakita A, Fujii M (2019) G3BP1 inhibits ubiquitinated protein aggregations induced by p62 and USP10. *Sci Rep* 9: 12896
- Bhaskar A, Kumar S, Khan MZ, Singh A, Dwivedi VP, Nandicoori VK (2020) Host sirtuin 2 as an immunotherapeutic target against tuberculosis. *Elife* 9: e55415
- Cao L, Yang G, Gao S, Jing C, Montgomery RR, Yin Y, Wang P, Fikrig E, You F (2019) HIPK2 is necessary for type I interferon-mediated antiviral immunity. *Sci Signal* 12: eaau4604
- Cheng S-T, Ren J-H, Cai X-F, Jiang H, Chen J (2018) HBx-elevated SIRT2 promotes HBV replication and hepatocarcinogenesis. *Biochem Biophys Res Commun* 496: 904–910
- Choi SJ, Lee HC, Kim JH, Park SY, Kim TH, Lee WK, Jang DJ, Yoon JE, Choi YI, Kim S et al (2016) HDAC6 regulates cellular viral RNA sensing by deacetylation of RIG-I. *EMBO J* 35: 429–442
- Dai J, Huang YJ, He X, Zhao M, Wang X, Liu ZS, Xue W, Cai H, Zhan XY, Huang SY et al (2019) Acetylation blocks cGAS activity and inhibits self-DNA-induced autoimmunity. *Cell* 176: 1447–1460
- Di Domizio J, Gulen MF, Saidoune F, Thacker VV, Yatim A, Sharma K, Nass T, Guenova E, Schaller M, Conrad C et al (2022) The cGAS-STING pathway drives type I IFN immunopathology in COVID-19. *Nature* 603: 145–151
- Dryden SC, Nahhas FA, Nowak JE, Goustin AS, Tainsky MA (2003) Role for human SIRT2 NAD-dependent deacetylase activity in control of mitotic exit in the cell cycle. *Mol Cell Biol* 23: 3173–3185
- Du M, Chen ZJ (2018) DNA-induced liquid phase condensation of cGAS activates innate immune signaling. *Science* 361: 704–709
- Eskandarian HA, Impens F, Nahori MA, Soubigou G, Coppee JY, Cossart P, Hamon MA (2013) A role for SIRT2-dependent histone H3K18 deacetylation in bacterial infection. *Science* 341: 1238858
- Fitzgerald KA, McWhirter SM, Faia KL, Rowe DC, Latz E, Golenbock DT, Coyle AJ, Liao SM, Maniatis T (2003) IKKepsilon and TBK1 are essential components of the IRF3 signaling pathway. *Nat Immunol* 4: 491–496
- Gal J, Chen J, Na DY, Tichacek L, Barnett KR, Zhu H (2019) The acetylation of lysine-376 of G3BP1 regulates RNA binding and stress granule dynamics. *Mol Cell Biol* 39: e00052-19
- Gao D, Li T, Li XD, Chen X, Li QZ, Wight-Carter M, Chen ZJ (2015) Activation of cyclic GMP-AMP synthase by self-DNA causes autoimmune diseases. *Proc Natl Acad Sci USA* 112: E5699–E5705
- Gogoi M, Chandra K, Sarikhani M, Ramani R, Sundaresan NR, Chakravorty D (2018) Salmonella escapes adaptive immune response via SIRT2 mediated modulation of innate immune response in dendritic cells. *PLoS Pathog* 14: e1007437
- Guillén-Boixet J, Kopach A, Holehouse AS, Wittmann S, Jahnel M, Schlüßler R, Kim K, Trussina I, Wang J, Mateju D et al (2020) RNA-induced conformational switching and clustering of G3BP drive stress granule assembly by condensation. *Cell* 181: 346–361
- Hamaidi I, Zhang L, Kim N, Wang MH, Iclozan C, Fang B, Liu M, Koomen JM, Berglund AE, Yoder SJ et al (2020) Sirt2 inhibition enhances metabolic fitness and effector functions of tumor-reactive T cells. *Cell Metab* 32: 420–436
- He M, Chiang HH, Luo H, Zheng Z, Qiao Q, Wang L, Tan M, Ohkubo R, Mu WC, Zhao S et al (2020) An acetylation switch of the NLRP3 inflammasome regulates aging-associated chronic inflammation and insulin resistance. *Cell Metab* 31: 580–591
- Jiao F, Wang Y, Zhang W, Zhang H, Chen Q, Wang L, Shi C, Gong Z (2020) AGK2 alleviates lipopolysaccharide induced neuroinflammation through regulation of mitogen-activated protein kinase phosphatase-1. *J Neuroimmune Pharmacol* 15: 196–208
- Jing E, Gesta S, Kahn CR (2007) SIRT2 regulates adipocyte differentiation through FoxO1 acetylation/deacetylation. *Cell Metab* 6: 105–114
- Jing H, Zhang X, Wisner SA, Chen X, Spiegelman NA, Linder ME, Lin H (2017) SIRT2 and lysine fatty acylation regulate the transforming activity of K-Ras4a. *Elife* 6: e32436
- Kato H, Takeuchi O, Sato S, Yoneyama M, Yamamoto M, Matsui K, Uematsu S, Jung A, Kawai T, Ishii KJ et al (2006) Differential roles of MDA5 and RIG-I helicases in the recognition of RNA viruses. *Nature* 441: 101–105
- Kim HS, Vassilopoulos A, Wang RH, Lahusen T, Xiao Z, Xu X, Li C, Veenstra TD, Li B, Yu H et al (2011) SIRT2 maintains genome integrity and suppresses tumorigenesis through regulating APC/C activity. *Cancer Cell* 20: 487–499
- Kim SS, Sze L, Liu C, Lam KP (2019) The stress granule protein G3BP1 binds viral dsRNA and RIG-I to enhance interferon-beta response. *J Biol Chem* 294: 6430–6438
- Kim Y-Y, Hur G, Lee SW, Lee S-J, Lee S, Kim S-H, Rho M-C (2020) AGK2 ameliorates mast cell-mediated allergic airway inflammation and fibrosis by inhibiting FcεRI/TGF-β signaling pathway. *Pharmacol Res* 159: 105027
- Krishnan J, Danzer C, Simka T, Ukropec J, Walter KM, Kumpf S, Mirtschink P, Ukropcova B, Gasperikova D, Pedrazzini T et al (2012) Dietary obesity-associated Hif1alpha activation in adipocytes restricts fatty acid oxidation and energy expenditure via suppression of the Sirt2-NAD<sup>+</sup> system. *Genes Dev* 26: 259–270
- Kwon S, Zhang Y, Matthias P (2007) The deacetylase HDAC6 is a novel critical component of stress granules involved in the stress response. *Genes Dev* 21: 3381–3394
- Li Y, Nie H, Wu D, Zhang J, Wei X, Ying W (2013) Poly(ADP-ribose) polymerase mediates both cell death and ATP decreases in SIRT2 inhibitor AGK2-treated microglial BV2 cells. *Neurosci Lett* 544: 36–40
- Liu J, Qian C, Cao X (2016) Post-translational modification control of innate immunity. *Immunity* 45: 15–30
- Liu ZS, Cai H, Xue W, Wang M, Xia T, Li WJ, Xing JQ, Zhao M, Huang YJ, Chen S et al (2019) G3BP1 promotes DNA binding and activation of cGAS. *Nat Immunol* 20: 18–28
- Muñoz-Sánchez J, Cháñez-Cárdenas ME (2019) The use of cobalt chloride as a chemical hypoxia model. *J Appl Toxicol* 39: 556–570
- Outeiro TF, Kontopoulos E, Altmann SM, Kufareva I, Strathearn KE, Amore AM, Volk CB, Maxwell MM, Rochet JC, McLean PJ et al (2007) Sirtuin 2 inhibitors rescue alpha-synuclein-mediated toxicity in models of Parkinson's disease. *Science* 317: 516–519
- Peck B, Chen CY, Ho KK, Di Fruscia P, Myatt SS, Coombes RC, Fuchter MJ, Hsiao CD, Lam EW (2010) SIRT inhibitors induce cell death and p53 acetylation through targeting both SIRT1 and SIRT2. *Mol Cancer Ther* 9: 844–855
- Pereira JM, Chevalier C, Chaze T, Gianetto Q, Impens F, Matondo M, Cossart P, Hamon MA (2018) Infection reveals a modification of SIRT2 critical for chromatin association. *Cell Rep* 23: 1124–1137
- Piracha ZZ, Kwon H, Saeed U, Kim J, Jung J, Chwae YJ, Park S, Shin HJ, Kim K (2018) Sirtuin 2 isoform 1 enhances hepatitis B virus RNA transcription and DNA synthesis through the AKT/GSK-3beta/beta-catenin signaling pathway. *J Virol* 92: e00955-18
- Qiao Y, Zhu S, Deng S, Zou SS, Gao B, Zang G, Wu J, Jiang Y, Liu YJ, Chen J (2020) Human cancer cells sense cytosolic nucleic acids through the RIG-I-MAVS pathway and cGAS-STING pathway. *Front Cell Dev Biol* 8: 606001

- Rao P, Suvas S (2019) Development of inflammatory hypoxia and prevalence of glycolytic metabolism in progressing herpes stromal keratitis lesions. *J Immunol* 202: 514–526
- Rothgiesser KM, Erener S, Waibel S, Luscher B, Hottiger MO (2019) Correction: SIRT2 regulates NF-kappaB-dependent gene expression through deacetylation of p65 Lys310 (doi:10.1242/jcs.073783). *J Cell Sci* 132: jcs232801
- Stetson DB, Ko JS, Heidmann T, Medzhitov R (2008) Trex1 prevents cell-intrinsic initiation of autoimmunity. *Cell* 134: 587–598
- Su CI, Kao YT, Chang CC, Chang Y, Ho TS, Sun HS, Lin YL, Lai MMC, Liu YH, Yu CY (2020) DNA-induced 2'3'-cGAMP enhances haplotype-specific human STING cleavage by dengue protease. *Proc Natl Acad Sci USA* 117: 15947–15954
- Sun W, Li Y, Chen L, Chen H, You F, Zhou X, Zhou Y, Zhai Z, Chen D, Jiang Z (2009) ERIS, an endoplasmic reticulum IFN stimulator, activates innate immune signaling through dimerization. *Proc Natl Acad Sci USA* 106: 8653–8658
- Sun L, Wu J, Du F, Chen X, Chen ZJ (2013) Cyclic GMP-AMP synthase is a cytosolic DNA sensor that activates the type I interferon pathway. *Science* 339: 786–791
- Tang JL, Yang Q, Xu CH, Zhao H, Liu YL, Liu CY, Zhou Y, Gai DW, Pei RJ, Wang Y et al (2021) Histone deacetylase 3 promotes innate antiviral immunity through deacetylation of TBK1. *Protein Cell* 12: 261–278
- Vincent J, Adura C, Gao P, Luz A, Lama L, Asano Y, Okamoto R, Imaeda T, Aida J, Rothamel K et al (2017) Small molecule inhibition of cGAS reduces interferon expression in primary macrophages from autoimmune mice. *Nat Commun* 8: 750
- Wan Y, Wu W, Zhang J, Li L, Wan Y, Tang X, Chen X, Liu S, Yao X (2021) Tenovin-1 inhibited dengue virus replication through SIRT2. *Eur J Pharmacol* 907: 174264
- Wang F, Nguyen M, Qin FX, Tong Q (2007) SIRT2 deacetylates FOXO3a in response to oxidative stress and caloric restriction. *Aging Cell* 6: 505–514
- Wu J, Sun L, Chen X, Du F, Shi H, Chen C, Chen ZJ (2013) Cyclic GMP-AMP is an endogenous second messenger in innate immune signaling by cytosolic DNA. *Science* 339: 826–830
- Xu Y, Li F, Lv L, Li T, Zhou X, Deng CX, Guan KL, Lei QY, Xiong Y (2014) Oxidative stress activates SIRT2 to deacetylate and stimulate phosphoglycerate mutase. *Cancer Res* 74: 3630–3642
- Yang W, Ru Y, Ren J, Bai J, Wei J, Fu S, Liu X, Li D, Zheng H (2019) G3BP1 inhibits RNA virus replication by positively regulating RIG-I-mediated cellular antiviral response. *Cell Death Dis* 10: 946
- Yang P, Mathieu C, Kolaitis RM, Zhang P, Messing J, Yurtsever U, Yang Z, Wu J, Li Y, Pan Q et al (2020a) G3BP1 is a tunable switch that triggers phase separation to assemble stress granules. *Cell* 181: 325–345
- Yang W, Chen W, Su H, Li R, Song C, Wang Z, Yang L (2020b) Recent advances in the development of histone deacetylase SIRT2 inhibitors. *RSC Adv* 10: 37382–37390
- Yeh YH, Hsiao HF, Yeh YC, Chen TW, Li TK (2018) Inflammatory interferon activates HIF-1 $\alpha$ -mediated epithelial-to-mesenchymal transition via PI3K/AKT/mTOR pathway. *J Exp Clin Cancer Res* 37: 70
- Yu HB, Jiang H, Cheng ST, Hu ZW, Ren JH, Chen J (2018) AGK2, a SIRT2 inhibitor, inhibits hepatitis B virus replication *in vitro* and *in vivo*. *Int J Med Sci* 15: 1356–1364
- Yum S, Li M, Fang Y, Chen ZJ (2021) TBK1 recruitment to STING activates both IRF3 and NF-kappaB that mediate immune defense against tumors and viral infections. *Proc Natl Acad Sci USA* 118: e2100225118
- Zhang Y, Chi D (2018) Overexpression of SIRT2 alleviates neuropathic pain and neuroinflammation through deacetylation of transcription factor nuclear factor-kappa B. *Inflammation* 41: 569–578
- Zhang C, Shang G, Gui X, Zhang X, Bai XC, Chen ZJ (2019) Structural basis of STING binding with and phosphorylation by TBK1. *Nature* 567: 394–398
- Zhao Y, Yang J, Liao W, Liu X, Zhang H, Wang S, Wang D, Feng J, Yu L, Zhu W-G (2010) Cytosolic FoxO1 is essential for the induction of autophagy and tumour suppressor activity. *Nat Cell Biol* 12: 665–675
- Zhao M, Xia T, Xing JQ, Yin LH, Li XW, Pan J, Liu JY, Sun LM, Wang M, Li T (2022) The stress granule protein G3BP1 promotes pre-condensation of cGAS to allow rapid responses to DNA. *EMBO Rep* 23: e53166